Modelling cross-shore shoreline change on multiple timescales and their interactions

R.B. Schepper[1,2], R. Almar[3], E.W.J. Bergsma[4,5], S. de Vries[1], A.J.H.M. Reniers[1], M.A. Davidson [6], K.D. Splinter [7]

[1]Delft University of Technology, Faculty of Civil Engineering and Geosciences, Hydraulic Engineering Section, P.O. Box 5048, 2600 GA Delft, The Netherlands
[2]International Marine and Dredging Consultants (IMDC), Van Immerseelstraat 66, B-2018 Antwerp, Belgium
[3]IRD-LEGOS, UMR 5566, OMP, 14 Av. Edouard Belin, 31400, Toulouse, France
[4]CNES-LEGOS, UMR 5566, OMP, 14 Av. Edouard Belin, 31400, Toulouse, France
[5]CNES, Earth Observation lab, 18 Av. Edouard Belin, 31400, Toulouse, France
[6]University of Plymouth, School of Biological and Marine Sciences, Drake Circus, Plymouth, Devon, PL8 4AA, United Kingdom
[7]Water Research Laboratory, School of Civil and Environmental Engineering, UNSW Sydney, Sydney, New South Wales, Australia

Key Points:

- Implementation of multiple shoreline response factors to consider different timescales and their interplay in equilibrium shoreline models.
- Extreme forcing events can have a persistent impact on the longer term state of the beach.
- The long term shoreline location can modulate extreme event impacts.

Corresponding author: Rob Schepper, `robschepper@msn.com`

Abstract
Understanding and predicting shoreline changes is paramount to coastal managers to anticipate potential threats. These shoreline changes are often driven by complex processes at multiple timescales. In this paper, a new approach to model wave-driven, cross-shore shoreline change incorporating multiple timescales is introduced. As a base we use the equilibrium shoreline prediction model ShoreFor that accounts for a single timescale only. High resolution data collected at four distinctly different study-sites is used to train the new data driven model. The four data-sets together cover sites that are mid latitude storm-dominated, under the influence of tropical cyclones and monsoons, and equatorial storm-free dominated by seasonal climate variability. In addition to the direct forcing approach used in most models, here two additional terms are introduced: 1) a time-upscaling and 2) a time-downscaling approach. The upscaling approach accounts for the persistent effect of short term events, such as storms, on the shoreline position. The downscaling approach accounts for the effect of long term shoreline modulation on shorter event impacts. The multi-timescale model shows considerable improvement compared to the direct-forcing approach in the original ShoreFor model at the four contrasted sites.

1 Introduction

Sandy beaches are constantly adapting to changing wave forcing over a variety of temporal scales (Larson & Kraus, 1995; Pianca et al., 2015; Almar et al., 2017), which can be traced in cross-shore shoreline changes. Coastal variability, and particularly erosion, can expose human- and ecosystems in the littoral zone to risk, which implies that understanding and predicting shoreline evolution is of paramount importance. However, it is not straightforward to predict shoreline variability at a multitude of natural temporal scales from storm events to seasonal and inter-annual evolution due to intrinsic limitations of current observation strategies. These observational strategies generally focus on a particular spatial-temporal scale (Plant et al., 2007; Bergsma & Almar, 2020). The same is true for many of the equilibrium-based shoreline models (Montaño et al., 2020) that are optimized during the calibration process for the single most dominant timescale of shoreline variability in the training set. Quite often this results in models being skillful at either the short-term (storm) timescale or optimized for the longer (seasonal to inter-annual) timescales. Addressing all the timescales together is a major challenge and as a result, current understanding on how the shorelines respond to different timescales and how these timescales influence shoreline change is limited. In addition to these temporal limitations, spatial restrictions exist. Most of the research on shoreline change over the last decades has been conducted at storm-dominated mid-latitudes, obscuring understanding to various mechanisms that play a role at different latitudes (e.g Takbash & Young, 2019). In the mid-latitudes, winter storms or the seasonality in the storms dominate the wave regime. Conversely, in the Tropics seasonal monsoons can dominate the wave climate and shoreline changes instead of paroxysmal storms such as tropical cyclones. At the equator, storm-free coasts are seen, where inter-annual changes of wave regimes predominate. In the two latter areas, climate modes exert a strong modulation of waves on inter-annual-, seasonal- and event-timescales such as tropical cyclones or monsoon pulses (Ondoa et al., 2017; Marchesiello et al., 2020).

Recent studies identified the persistent nature of short wave events on longer beach response timescales (Frazer et al., 2009; Anderson et al., 2010; Karunarathna et al., 2014; Angnuureng et al., 2017; Almar et al., 2017). This link between the different timescales is often missing when modelling the seasonal to inter-annual evolution of the coastline and storm impact persistence. For example, extremes (e.g.

storms and tropical cyclones) have both transient and persistent impact, individually or in sequence (Anderson et al., 2010). Moreover, Angnuureng et al. (2017) showed the influence of average winter storms on beach response and revealed that not only the storm energy is important, but also the frequency of recurrence, highlighting interactions between short-term storms and long-term evolution. They showed the importance of the recurrence-frequency of extremes to beach erosion and post-event reconstruction; such that the shoreline retreat was most governed by the first storm in the sequence, while the impact of subsequent forcing events was less pronounced (low cumulative impact), something that is also observed in Bergsma et al. (2019) and follows the general equilibrium response of a beach (Yates et al., 2009; Davidson et al., 2013; Splinter et al., 2014). Furthermore, a main outcome of recent studies in tropical South East Asia (Almar et al., 2017; Thuan et al., 2019) is the long lag (50–60 days) observed between monthly-averaged waves and shoreline location, while the envelope of intra-seasonal monsoon events is in closer phase with the shoreline location. Hence, the shoreline variation appears to be in equilibrium with energetic wave conditions, rather than the monthly-averaged waves. This is in line with observations by Jackson et al. (2002) at low-energy environments where the beach is assumed to be in equilibrium with previous energetic wave events rather than with current conditions. The beach is considered inactive the rest of the time. It is the particularly long duration of winter monsoon events that presumably drive most of the shoreline changes, with very gentle wave conditions in between which limit the recovery potential, as observed elsewhere.

The understanding and prediction of coastal evolution is often simulated using models that simulate hydrodynamics linked to morphodynamics that can roughly be divided into three categories: the more complex and time-consuming process-based models (Walstra et al., 2012, 2016; Callaghan et al., 2013; Roelvink et al., 2009), hybrid models (usually based on the equilibrium concept (Montaño et al., 2020)) and more recently, machine learning models (Goldstein et al., 2019). Each of these models are typically bound to the dominant spatial- and temporal scales of key processes to model, and as a result they struggle, or become too computational expensive, to account for dynamics at different timescales. Hybrid (equilibrium) models are generally more computationally efficient in comparison to process-based models and have been proven reliable on inter-annual timescales to simulate shoreline behaviour (Miller & Dean, 2004; Yates et al., 2009; Davidson et al., 2013; Splinter et al., 2014; Splinter et al., 2017). However, they typically account for a single dominant physical process and need a large, site-specific, dataset for calibration purposes (Splinter et al., 2013). A limitation to these models however, is that only coastal processes observed during the calibration time-frame are accounted for (Vitousek et al., 2017). Moreover, hybrid models do not explicitly account for all individual processes that drive shoreline change but seek an overall behaviour pattern as response to the different processes.

In this paper we evaluate to what extent multiple timescales of dominant forcing- and beach response behavior co-exist and to what extent such behaviors can interact with different timescales of forcing and response. We aim to improve cross-shore multi-timescale shoreline predictions by using the single timescale ShoreFor model (SF-ST, see Appendix A for a model description) as a baseline model. The research uses data from four datasets with contrasting timescales and characteristics.

2 Model training sites covering different wave environments

To train the SF-ST model, shoreline location and wave measurements are required. A source of shoreline data are shore-based video cameras that generally collect data during daylight on a 30-min basis (Holman & Stanley, 2007). In comparison to shoreline-walking GPS surveys, these video-based shorelines provide significantly better temporal resolution, which makes video-derived shorelines particularly suitable to study the importance of different, multiple, response timescales (Ondoa et al., 2020; Pianca et al., 2015).

In order to make the video-data suitable for SF-ST and to cover a wide range of timescales (1 day to inter-annual timescales), all shoreline and wave forcing datasets are interpolated (upsampled, corresponding to the value every 24-hours), such that they have a temporal resolution of 1 day. Moreover, the raw shoreline position data is detrended by a second order polynomial, to filter out shoreline trends which have a larger temporal scale than the duration of the dataset. The importance of multiple beach response timescales will be investigated at four different study sites: Narrabeen (Australia), Nha Trang (Vietnam), Tairua (New Zealand) and Grand Popo (Benin). These sites were chosen to cover different wave environments and for the availability of daily shoreline data. All four beaches are subjected to a small tidal range (microtidal, <2.0 m, <1.6 m, <2.0 m and <1.8 m, respectively), such that SF-ST has an optimal model performance (Harley et al., 2011; Almar et al., 2017; Blossier et al., 2017; Ondoa et al., 2017), respectively. Moreover, the beach dynamics are either dominated or largely influenced by cross-shore processes. Furthermore, major differences between the wave conditions are present at the four study sites. The wave climate at Narrabeen consists of small (daily) timescale storms (and swell waves) and a larger temporal scale, but less intense seasonal cycle. At Nha Trang, three distinct wave forcing timescales are present: typhoons (daily), monsoons (monthly) and a seasonal variation (annual). At Tairua, the wave climate is largely influenced by small timescale storm- and swell waves (Bradshaw et al., 1991). At Grand Popo two timescales in the wave forcing are present: on the one hand, wind- and swell waves (daily) and on the other hand a considerable seasonal variation.

2.1 Narrabeen-Collaroy, Australia

The Narrabeen-Collaroy beach (34^0 S) is situated near Sydney in the southeast of Australia (Figure 1). The embayed beach is bound at the north and south by two headlands. Narrabeen beach is situated in the north of the embayment and Collaroy beach is situated in the south. In 2004, an ARGUS system (Holman & Stanley, 2007; Turner et al., 2016) was installed. In this paper, alongshore averaged shoreline data a bit southwards of the center of the embayment is used (2400 m to 2800 m from the northern edge of the embayment), in line with previous studies at this beach (Davidson et al., 2013; Phillips et al., 2017). Narrabeen beach is characterised by sand with a D50 of 0.4 mm. The wave climate is largely influenced by swells from the SSE (mean $H_s = 1.6$ m and mean $T_p = 10$ s). Additionally, the wave climate consists of larger waves ($H_s = 3$ m) that originate from storm events and can hit the coastline in any direction. Furthermore, a small seasonal cycle is present with on average higher waves in the Australian winter- and milder waves in the Australian summer months (Davidson et al., 2017). On larger timescales, effects of El-Nino Southern Oscillation (ENSO) can play a role as well (Turner et al., 2016; Ranasinghe et al., 2004; Harley et al., 2009). In this study, nearshore wave time-series at the 10 m depth contour are used.

2.2 Nha-Trang beach, Vietnam

A video system (Lefebvre et al., 2014; Thuan et al., 2016) was installed in 2013 at Nha Trang beach in Vietnam (12^0 N) (Figure 1). The camera location is considered far enough for the beach not to be influenced by the edges of the bay (Almar et al., 2017). Cross-shore shoreline positions are estimated from this camera data on a daily basis. The shoreline location used in this paper is retrieved by

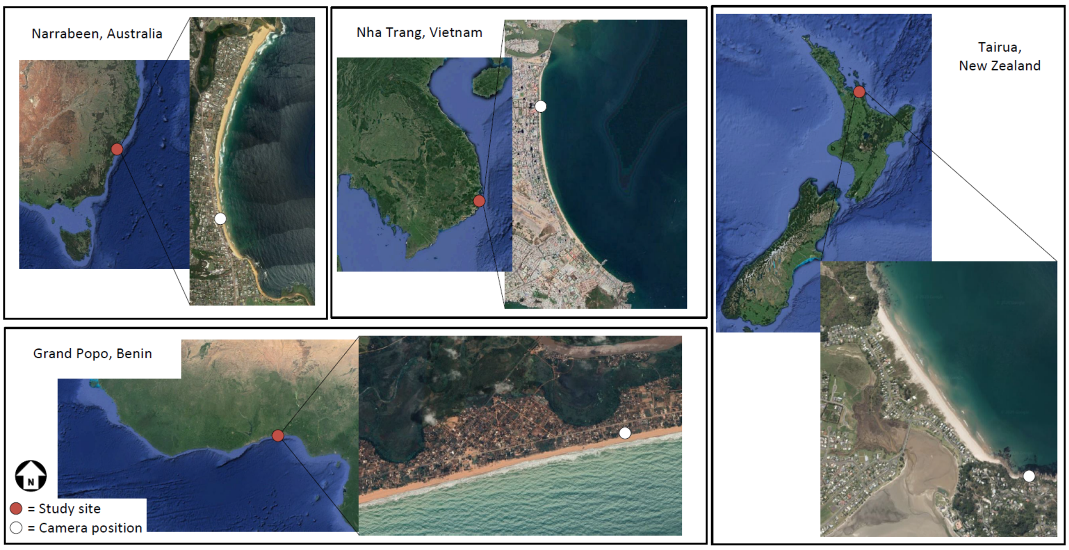

Figure 1. Overview of the model training sites and positions of the camera-stations from which high-resolution shoreline data is extracted. Top left: Narrabeen- and Colleroy beach embayment. Top center: the Nha Trang beach in Vietnam. Bottom left: Grand Popo beach in Benin. Right: Tairua beach in New Zealand.

alongshore averaging the video-derived shoreline data (over 75 m) from the northern part of the bay relative to the camera location. Nha Trang beach is characterised by sand with a D50 of 0.3 mm. Interestingly, the tropical wave climate at Nha Trang is characterized by multiple wave conditions with a distinct timescale, of which the seasonal variation is the most pronounced. The offshore annual mean significant wave height H_s is 0.95 m, with an associated averaged peak period T_p of 6.2 s. Typhoons typically occur on average 4-6 times per year between August and November. The wave climate is also characterized by summer- and winter monsoons, where the summer monsoons mainly consist of wind waves and the winter monsoons of swell waves. The winter monsoons (October to April), which do not occur at the same time as the typhoons, can generate waves up to 4.0 m, which can heavily affect shoreline change. During fall and winter (October to April) the mean H_s is 1.2 m and T_p is 6.8 s, while during spring and summer (May to September) the mean H_s is reduced to 0.6 m with a shorter T_p below 5 s (Thuan et al., 2019).

2.3 Tairua beach, New-Zealand

Tairua Beach is situated at the east coast of New Zealand's northern island (37^0 S) (Figure 1). This 1.2 km long beach is situated in between two headlands, where on the southern headland a video camera was installed in 1998. In this study, high resolution shoreline data (alongshore averaged over the bay: 1050 m, see Montaño et al. (2020)) is used, which is extracted from those camera images. Tairua beach is characterised by sand with a D50 of 0.3 mm. The beach is subjected to easterly and northeasterly swell and storm waves (Blossier et al., 2017). The offshore wave climate has a mean H_s of 1.4 m, with up to 6 m during storm events (Smith & Bryan, 2007).

2.4 Grand Popo beach, Benin

A video system was installed in 2013 at Grand Popo (6^0 N), Benin, situated in the equatorial Gulf of Guinea, West Africa (Figure 1). It is an open-ocean, sandy stretch of coast which is situated far from any anthropological influences. The nearest one (20 km updrift) is a field of groynes, constructed in the last five years (Ondoa et al., 2020; Anthony et al., 2019). Grand Popo beach is characterised by sand with a D50 of 0.6 mm. Overall, the Gulf of Guinea can be considered as a storm free region with only distant swells and wind seas locally generated in the tropical band (6^0 N to 15^0 S) (annual mean $H_s = 1.36$ m, $T_p = 9.4$ s). Beach dynamics are dominated by long swells that originate from the southern hemisphere at high latitudes (Almar et al., 2015). Therefore, the wave climate consists of clear seasonal (and inter-annual) variations, with more energetic waves during the April-October period and less energetic waves during the November-March period.

3 Implementing multiple timescales and links between timescales in cross-shore shoreline model

We propose four steps to implement multiple dominant forcing and beach response timescales within the SF-ST model and to assess its performance. The first step is to distinguish timescales in the measured data using a filter function and subsequently determine which timescales are dominant in the raw forcing and shoreline position signals (Section 3.1). Then an approach to implement these multiple dominant timescales in the SF-ST model is proposed (Section 3.2). This implementation uses a threefold correspondence between the isolated timescales of the wave data to the isolated timescales in shoreline data where the timescales that are smaller, identical or larger are linked in a direct forcing, upscaling and downscaling procedure (Sections 3.2.1, 3.2.2 & 3.2.3, respectively). The combined model is referred to as ShoreFor Multiple Timescales (SF-MT). Subsequently, the modelling calibration and validation phases are elaborated in Section 3.3. In Appendix B model skill assessment and performance is discussed.

3.1 Distinguishing multiple timescales

To distinguish timescales, the raw shoreline position and wave forcing (H_s, T_p) data is filtered using a running average filter with varying (enlarging) window sizes. The running average filter is used to allow for data-gaps in the datasets. Per window, and hence timescale (i.e. 1 until the length of the time-series, with steps of 1 day), a residual variance of the shoreline position and wave forcing time-series is calculated. With residual variance of the filtered signals a temporal spectrum is constructed. In other words, we can plot the temporal spectrum as the (remaining) variance of all filtered signals as a function of the timescale. Dominant timescales are defined by the largest variance. In contrast to, for example Fourier spectra, the linear superposition of all filtered signals is not equal to the raw signal since the filter function is shape-preserving but not energy-conserving. By dividing the filtered signals by a weighting value proportional to the window size of the running average filter, energy is conserved and the raw signal can be reconstructed through linear superposition. As a consequence, the energy (i.e. variability) for each filtered signal reduces, where the difference is largest for the largest timescales, because the window width increases with increasing timescales. A second temporal spectrum can be constructed from the resulting signals, which is used to construct timescale-clusters by dividing the spectrum into bins (i.e. bands).

When filtered wave-forcing and shoreline position signals are directly related (i.e. on a corresponding timescale) using SF-ST, the corresponding calibration parameters and resulting modelled shoreline position signals are partly dependent on the variability of the related (input) signals. For example, the response value (i.e. c, Equation A1), becomes smaller if the variability of the wave forcing becomes larger (for the same shoreline signal), because the rate parameter (c) and wave energy flux (P) determine the magnitude of the shoreline response (Splinter et al., 2014). Hence, the variability of all (filtered) input signals has to be identical, when considering an inter-comparison of modelled shoreline position signals on multiple timescales. Therefore, timescale-clusters are used of which each cluster has an identical variability. To that end, the previously obtained spectrum is employed and will determine the number of timescale-clusters that is used for the multi-timescale implementation. Timescale-clusters are formed by dividing the obtained temporal spectrum into bins. Within such a bin a particular number of filtered signals can be found. The linear superposition of all filtered signals within a bin results in a time-series which represents a particular timescale (i.e. a timescale-cluster). The bin-distribution is based on an equal amount of shoreline response variation within each bin. In this way, all resulting timescale-clusters, which represent certain timescales, will have the same variance. The variability within a bin is equal to the signal with the largest variability in the spectrum, otherwise the variability of that signal does not fit within the bin. This means that only one filtered signal fits within the bin at the point corresponding to the peak of the spectrum. For other bins, multiple filtered signals can fit in a bin, because the variability of those individual signals is lower. The lower the variability of the spectrum, the wider the bins, the more filtered signals fit within a bin. Hence, the bin distribution is determined by adding up filtered signals (starting with the signal that has a timescale of 1 day), until that summation reaches the maximum variability of the bins. For the remaining filtered signals, a new bin is used. This procedure is continued up to the point where all filtered signals fall within a bin.

In the wave forcing spectra (i.e. the individual spectra for H_s and T_p), an identical bin-distribution is used as such that corresponding timescale-clusters are formed. Thereafter, the different timescale-clusters in the wave forcing data (H_s and T_p) are related to ones in the shoreline data on multiple scales. The interactions between the wave forcing and shoreline position timescale-clusters on multiple timescales are based on three approaches: the direct forcing-, the upscaling- and downscaling approach. The combined model is referred to as ShoreFor Multiple Timescales (SF-MT).

3.2 Implementing multiple timescales

In this section the multi-timescale implementation within the SF-ST model is governed by introducing the three separate terms: the direct forcing-, upscaling- and downscaling approach (Section 3.2.1, 3.2.2, 3.2.3, respectively). The direct forcing approach relates corresponding timescale-clusters in the wave and shoreline position data. The upscaling approach accounts for the persistent effect of short wave events on the shoreline position. The downscaling approach accounts for the effect of the longer timescales in beach variation on the impact to shorter forcing events by introducing a time-dependent response factor.

3.2.1 Direct Forcing

In the direct forcing approach all timescale-clusters in the wave forcing data (H_s & T_p) are related to corresponding timescale-clusters in the shoreline position data, following:

$$\frac{dx_i}{dt} = c(F(\phi)_i^+ + rF(\phi)_i^-) \tag{1}$$

in which i is an indicator of the fact that corresponding timescale-clusters are linked to each other. Note that the standard single timescale ShoreFor model (SF-ST, see Appendix A) is adapted in the direct forcing approach (except for the linear trend term), but it is applied multiple times: for each timescale-cluster with a distinct timescale. The linear trend term (b) is omitted from the model, because otherwise a linear trend will be present for every predicted shoreline signal (for every band). Within each band, no linear trend is present as the filter function only captures timescales which are smaller than the full length of the dataset. Hence, b should be zero when the full time-frame is considered. However, during the calibration phase only part of the entire dataset is used such that a (small) trend can be present. Subsequently, this trend will be assigned to b. As this linear trend will be extrapolated during the validation phase, it will result in a wrong shoreline prediction as no trend is present over the full period.

3.2.2 Upscaling: the long-term persistence of short-timescales

To include the relation between small wave forcing timescales and larger timescales in shoreline response, as small timescale wave forcing events (e.g. storms) can have a considerable and persistent effect on larger beach response timescales (e.g., Frazer et al., 2009; Anderson et al., 2010; Almar et al., 2017), an upscaling approach is proposed. This is described mathematically as follows:

$$\frac{dx_j}{dt} = c(F(\phi)^+_{i\to j} + rF(\phi)^-_{i\to j}) \tag{2}$$

wherein the subscript indices i and j indicate the timescales: i is the small timescale and j the larger one *($j>i$)*. The upscaling effect is indicated with an arrow. In this model improvement step the ShoreFor model equation has kept its original form (Equation A1), while only the forcing is represented differently.

This upscaling effect is evaluated by using an envelope (based on spline interpolation) of wave forcing timescale clusters that links the two different timescales. Figure 2 shows an example of an envelope (black-dashed) of a significant wave height timescale-cluster (black-solid), where it is clearly visible that the envelope has a larger timescale than the wave height signal. A similar approach is followed for the wave period. The envelopes representing the wave height and wave period will be related to the corresponding shoreline timescale-cluster (red-solid). The resulting modelled shoreline is represented by the red-dashed time-series in Figure 2.

3.2.3 Downscaling: the changing efficiency of short timescales due to long-term variations

The incorporation of the effect of large timescale shoreline variations on the efficiency with which smaller timescale wave-forcing events induce cross-shore sediment transport is achieved by a so-called downscaling approach. This step ensures that smaller beach response timescales can be accounted for, if larger ones dominate. The downscaling approach is compared to SF-ST slightly adapted and can be mathematically described as follows:

$$x_i(t) = c_j(t)\int_0^t (F(\phi,t)^+_i + rF(\phi,t)^-_i)dt \tag{3}$$

in which the subscript indices i and j indicate the timescales, where $j>i$. Downscaling can be further explained by the time-series in Figure 3. The dynamic

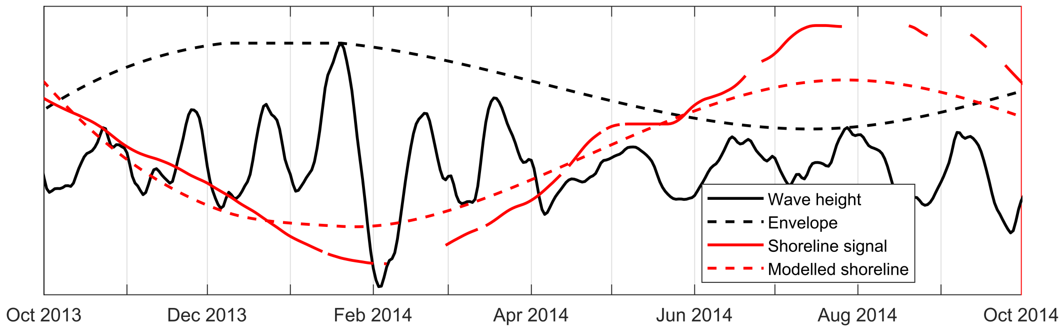

Figure 2. The upscaling approach: modelling the persistent effect of extreme forcing events on the longer term state of the beach. The effect of the small timescale wave height time-series (black-solid) on a larger shoreline position timescale (red-solid) is modelled using the envelope of the wave height time-series (black-dashed), which creates the timescale link. A similar approach is followed for the wave period. The resulting modelled shoreline is given by the dashed red line.

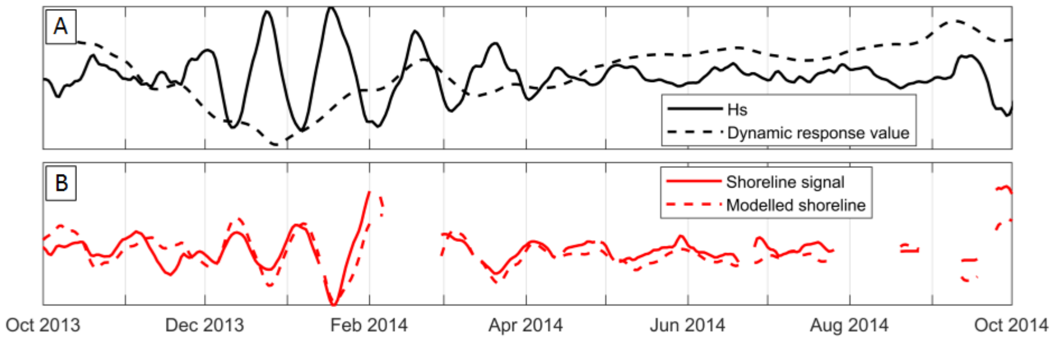

Figure 3. The downscaling approach: modelling the effect of long term shoreline trends on extreme event impacts. The solid black time-series represents the wave height. The effect of the larger timescales in shoreline variation on the efficiency with which smaller timescale wave-forcing events induce cross-shore sediment transport is modelled by using a dynamic response factor (black-dashed), which has the shape of the larger timescale shoreline variation signal. The shoreline signal with a smaller timescale is indicated by the solid red time-series and the resulting modelled shoreline signal is indicated by the red dashed line. Hence, if the shoreline on a larger timescale is accreted (e.g. October 2013, high dynamic response factor), the relative (compared to the wave forcing) shoreline response on a smaller timescale is large (higher sediment transport efficiency).

response factor ($c_j(t)$) (black-dashed) has the shape of the considered large timescale shoreline variation to account for a variable sediment transport efficiency, because beach response to small timescale high-intensity wave forcing events (red-solid) can depend on this larger timescale shoreline variation (i.e. the initial state of the beach). The figure shows that if the shoreline on a larger timescale is accreted (e.g. October 2013, high dynamic response factor), the relative (compared to the wave forcing, black-solid) shoreline response on a smaller timescale (red-solid) is large (higher sediment transport efficiency). Conversely, if it is eroded (e.g. January 2014, low dynamic response factor), the relative shoreline response is low (limited sediment transport efficiency). The resulting modelled shoreline time-series is indicated by the dashed red line in Figure 3B.

The justification of the downscaling approach consists of three components: 1) the influence of large timescale shoreline variations on beach response to small timescale high-intensity forcing events as observed in measurements, 2) modelling of small beach response timescales with the direct forcing approach and 3) modelling of small beach response timescales with the downscaling approach.

When a forcing event of a small temporal scale (e.g. storm/monsoon) impacts the coastline, the beach response can depend on whether that coastline is eroded or accreted on a larger temporal scale (e.g. due to a seasonal variation). Or stated otherwise, on the initial state of the beach (Aagaard et al., 2005). For a beach in the state of erosion, a minor retreat of the shoreline location is expected due to the presence of an erosion profile. For an accreted beach a larger beach response is expected. If the period between two similar high-intensity forcing events is very small compared to the calibrated memory decay factor ($<2\phi$), the direct forcing approach is already able to model the fact that the subsequent forcing events correspond to a different beach response. The (modelled) response to the second forcing event is lower, because the coastline is already closer to the equilibrium with the high-intensity forcing conditions. This is due to the dynamic equilibrium condition (Equation A4) which introduces a negative feedback mechanism: the disequilibrium between the present and the antecedent forcing is lower during the second forcing event. This mechanism ensures that if two high-intensity forcing events approach the coastline shortly after each other, the cumulative shoreline recession is limited (Davidson et al., 2013). However, if the period between two similar high-intensity forcing events is considerably larger than the memory decay factor ($>2\phi$), the direct forcing approach is not able to model a different beach response due to a different initial state of the beach (i.e. a varying shoreline on a larger timescale). Due to the constant response factor (i.e. c; Equation 1) and the large period between the two short high-intensity forcing events, the direct forcing approach will model two beach responses with the same erosional amplitude. Hence, no connection is present between the larger timescale shoreline variation and the modelled small timescale beach response to high-intensity forcing conditions.

To implement the dependency of small timescale beach response (to short high-intensity forcing events) on large timescale beach variations, a time-varying response factor is used (i.e. *c(t)*; Equation 3). This dynamic response factor represents the changing efficiency over time with which waves induce cross-shore sediment transport and is a function of the spatial separation between the shoreline and the offshore sediment source (e.g. sand bars(s)). This spatial separation normally scales with the surfzone width imposed by the antecedent waves, with lower response rates for erosion profiles (wide surfzone) due to the inefficient transfer of sediment between the offshore region and the beach face. Conversely, as the offshore sand supply is migrated closer to the shoreline (narrow surfzone; accreted beach), the sediment transport efficiency increases, facilitating faster response. Therefore, the dynamic response factor has the shape of a large timescale shoreline signal. Now, the response to a short high-intensity forcing event is higher (large sediment transport efficiency) when the beach (on a larger time scale) is accreted and lower (small efficiency) when the beach is already eroded.

3.3 Model calibration and validation

The modelling of cross-shore shoreline change on multiple timescales is divided in two phases: model calibration and model validation. During model calibration the site-specific model free parameters (c_i & ϕ_i) are determined using the wave forcing- ($H_{s,i}$ and $T_{p,i}$) and shoreline data ($x_{s,i}$), where the subscript i indicates the multiple predictions from the direct forcing-, upscaling- and downscaling approaches. At the time of model validation, wave forcing data is used as model input only and

Dataset	Calibration time-frame	Validation time-frame	Data-gaps shoreline position [%]
Narrabeen	01-08-2004 / 10-07-2010	11-07-2010 / 19-04-2015	25
Nha Trang	27-07-2013 / 31-12-2014	01-01-2015 / 01-11-2015	20
Tairua	02-01-1999 / 31-12-2008	01-01-2009 / 31-12-2013	0
Grand Popo	20-02-2013 / 22-11-2015	23-11-2015 / 22-06-2016	40

Table 1. Calibration- and validation time-frames of the Narrabeen-, Nha Trang-, Tairua and Grand Popo dataset, as well as the percentages of data-gaps in the shoreline position data (based on daily data).

together with the calibrated parameters shoreline predictions are generated. Table 1 presents the calibration and validation time-frames for all four datasets. Furthermore, note the difference in the percentages of data-gaps in the shoreline position data (the wave forcing data is continuous for all four study sites).

3.3.1 Calibration of the downscaling approach

While the calibration method for the direct forcing and upscaling approach is similar to that of the SF-ST model, the calibration method for the downscaling approach is slightly different considering that the dynamic response factor (*c(t)*) has the shape of a larger timescale shoreline signal. However, this dependency poses a problem as during validation the model must generate shoreline predictions which are solely based on wave forcing (shoreline data is not available). Hence, a different approach is needed to generate the shape of the dynamic response factor. To that end, note that the modelled signals from the direct forcing and upscaling approach are available before applying the downscaling approach and will therefore be used to capture the total shoreline response to come up with a shoreline signal. Subsequently, that shoreline signal will be filtered to generate timescale-clusters that can be used as dynamic response factors. However, during the direct forcing and upscaling approach multiple shoreline time-series with different timescales are generated (Equations 1 and 2) and not all those signals will equally contribute to the total shoreline change prediction at the considered site; some will have no contribution at all. Therefore, a linear least-squares solver with bounds is used (after the determination of the model free parameters) to find which summation of predicted shoreline signals fits best to the raw measured shoreline position data. The procedure can be written down in the following manner:

$$\min_{k} \frac{1}{2}||\mathbf{C} \cdot \underline{k} - \underline{d}||^2 \; with \; 0 \leq \underline{k} \leq 1 \tag{4}$$

In which the matrix $\mathbf{C}$ contains all the individual modelled shoreline signals (time-series) with a distinct timescale that are generated using the direct forcing and upscaling approach, $\underline{\mathrm{d}}$ the vector containing the measured shoreline data, the double vertical lines represent the mathematical norm and $\underline{\mathrm{k}}$ the calculated vector containing values between the lower (zero) and upper (one) bound. Individual modelled shoreline signals (resulting from Equations 1 and 2) which are not important for the total shoreline prediction attain a zero value, whereas the most important signals attain a value of one. The matrix $\mathbf{C}$ only contains modelled shoreline signals that have a relatively high correlation with the corresponding measured time-series. Modelled shoreline signals with a relatively low correlation (with the corresponding measured time-series) result from a poor relation between the wave forcing and shoreline data and are therefore not used. The thresholds indicating a low/high correlation are determined through the fitting of a normal distribution to all correlation values per model improvement step. The thresholds indicating a high correlation are set to an optimized probability of exceedance of 90%, for both the direct forcing and upscaling approach. This ensures that most signals will be used as input for the linear least-squares solver and only the poorest modelled shoreline signals are omitted. Subsequently, the resulting total shoreline signal is filtered and timescale-clusters are generated following the same bin-distribution as was used to determine the timescale-clusters for the direct forcing and upscaling approach. These timescale-clusters are used as the dynamic response factor, such that all shoreline predictions in the validation phase, using the three modelling approaches, can be generated by the wave forcing only. Note that this procedure implies that shoreline predictions generated with the downscaling approach are partly based on shoreline predictions generated with the direct forcing and upscaling approach.

3.3.2 Predicting the total shoreline change

Now, the procedure following Equation 4 is applied again, but with modelled shorelines of all three approaches. The thresholds were adapted, which resulted in the P90, P75 and P50 probability of exceedance for the direct forcing, upscaling and downscaling approach, respectively. The probability of exceedance is higher for the direct forcing approach as there are less shoreline signals generated using that approach (N in case of N timescale-clusters, while for the up- and downscaling approach $(N^2 - N)/2$ signals are generated). Note that the summation of modelled shoreline signals that will model the total shoreline change during the calibration phase ($\sum \mathbf{C} \cdot \underline{\mathrm{k}}$), is also responsible for modelling shoreline change during model validation ($\sum \mathbf{D} \cdot \underline{\mathrm{k}}$, where $\mathbf{D}$ is the matrix containing the individual predicted shoreline signals for the validation phase).

4 Results

In this section, calibration (Section 4.1) and validation (Section 4.2) results are presented, when SF-ST and the multi-timescale model (SF-MT) are applied to all four datasets. An overview of model results assessed by four different model skill indicators (correlation, NMSE, BSS & AIC), is presented in Section 4.3.

Table 2 provides information regarding the four datasets at the model training sites used in this study: Narrabeen, Nha Trang, Tairua & Grand Popo. The number of timescale bins is presented, which represents the number of timescale-clusters used in the multi-timescale implementation. Or stated otherwise, in how many bins the temporal spectra are divided. Note that at Grand Popo a limited number of timescale bins is used (i.e. 9): this is the maximum number of bins for which the requirement of identical shoreline variability within each bin (Section 3.1) can be met. The most striking difference between the datasets is the number of dominant timescales in the shoreline position and wave forcing data (i.e. local maximums in the temporal spectra, Section 3.1 and Figure C1).

At Narrabeen, only one dominant timescale is found in the shoreline position signal that is related to the seasonal variation (i.e. 322 days, Table 2). Besides the seasonal variation, the storm/swell timescale is dominant in the wave forcing data (i.e. 2-14 days). At Nha Trang, two dominant timescales are present in the wave forcing: the monsoon- and seasonal timescale, which implies that typhoons are not dominant. In the shoreline position signal, only the seasonal variation is dominant.

Dataset	Timescale bins	Dominant timescale shoreline position [days]	Dominant timescale wave forcing [days]
Narrabeen	45	322	2-14 & 350
Nha Trang	35	302	10-26 & 314-342
Tairua	23	34 & 434-806	2-10
Grand Popo	9	6 & 46 & 326	10 & 94 & 358

Table 2. Information of the Narrabeen-, Nha Trang-, Tairua and Grand Popo dataset. Dominant timescales are defined as local maximums in the temporal spectra (see Appendix C).

At Tairua, a monthly- and seasonal- to inter-annual timescale is dominant in the shoreline position signal, while storms/swells dominate the wave climate. At Grand Popo even more dominant timescales are found in the shoreline position data: a storm/swell-, an approximately monthly- and a seasonal timescale. In the wave forcing data three dominant timescales can be found as well: a storm/swell timescale, a timescale of approximately 3 months and a seasonal timescale.

4.1 Calibration

Figure 4 presents the results (calibration and validation) when SF-ST (black) and SF-MT (red) are applied to the datasets at Narrabeen (top), Nha Trang (second), Tairua (third) and Grand Popo (bottom). The transition between the calibration and validation time periods is indicated with a dashed black line. Figure 5 presents the contribution of each model improvement step over time (left, in similar order) and the corresponding relative contribution of each model improvement step (right) for the calibration period only. The blue, orange and purple lines correspond to the direct forcing, upscaling and downscaling approaches, respectively. In Figure 6 the standard deviation per timescale-cluster is shown (left panels) for the shoreline position data (green), the SF-ST (black) and SF-MT (red) model result (calibration + validation) for all datasets (in similar order as Figure 4 and 5). In the middle panel the correlation between the SF-MT model result (and SF-ST) and the shoreline position data is presented on all different timescales. In the right panels, a model score is given for each of the three model improvement steps for all different timescales. The score for every timescale consists of the correlation coefficient (model result - data on that particular timescale) multiplied by standard deviation of that modelled signal, timescale and model improvement step. Using this modelling result score means that 1) if the correlation between the data - model is high, the model is able to reproduce shoreline change at this timescale, 2) if the standard deviation of the model result is high, that particular shoreline signal is important in determining shoreline change according to Equation 4.

For the Narrabeen dataset (top panel in Figure 4) SF-ST (black) is able to capture the smaller timescale storm/swell response (order of days), but the larger timescale shoreline variations are captured to a lesser extent ($\phi = 3$ days and $c = 1.96 * 10^{-7}\ (m/s)/(W/m)^{0.5}$). The SF-MT model (red) also captures the storm timescale to a certain extent, but yields a considerable increase in skill (BSS of 0.61) by better capturing shoreline change on larger timescales (larger than the storm timescale). This occurs for example in 2009, where first the large erosion period halfway through 2009 is captured well by the SF-MT model and poorly by SF-ST, while the same occurs for the accretive period during the second half of 2009. Overall the SF-MT model yields a better fit to the data, compared to SF-ST, which seems to underestimate the amplitude of shoreline accretion/erosion most of the time. This is emphasized by the NMS error between the data and model result, which is 0.71 for SF-ST and reduces to 0.29 for the SF-MT model. This corresponds to a 'fair' and 'excellent' rating for SF-ST and SF-MT, respectively. The standard deviation and correlation plot per timescale (Figure 6A) shows that for storm/swell timescales (1-12 days) SF-ST has a higher standard deviation and a similar correlation. Hence, the smaller storm timescales are better captured by the SF-ST model. However, for SF-MT the standard deviation multiplied with the correlation is higher for timescales larger than 33 days (up to 2285 days). Hence, the dominant seasonal timescale is better captured by the SF-MT model, which contributes most to the model improvement. Moreover, the upscaling approach contributes considerably (73%) to the total shoreline signal (orange lines in Figure 5A). The larger timescales are captured by the upscaling and downscaling (purple, Figure 6A) approaches whereas the smaller (storm) timescales are captured by the downscaling approach as well. The direct forcing approach (blue) has a limited contribution to the total model result (7%, Figure 5A), compared to the upscaling (73%) and downscaling (20%) approach.

At Nha Trang considerable improvement is made by implementing multiple timescales within the SF-ST model (Figure 4B), which is emphasized by a BSS of 0.62 (i.e. an 'excellent' rating). Where SF-ST ($\phi = 180$ days and $c = 4.61 \quad * \quad 10^{-8}$ $(m/s)/(W/m)^{0.5}$) only partially captures the seasonal timescale (the most dominant timescale, see Table 2 and Figure C1), the SF-MT model captures both the response to monsoons and the seasonal variation in wave data (i.e. the two dominant timescales in the wave data). The NMS errors for SF-ST and SF-MT with the data is 0.31 ('good') and 0.13 ('excellent'), respectively. Figure 6B shows that the standard deviation and correlation per timescale for SF-MT (red) are high and relatively uniformly distributed across the different timescales. This states that all timescales are well captured. For SF-ST (black) the correlation is lower for all timescales except for the seasonal variation, where the correlation is similar. The standard deviation is lower/higher for timescales smaller/larger than 78 days. If both indicators are combined, it becomes clear that the largest contributor to the model improvement of SF-MT are the smaller timescales (i.e. the monsoons). Furthermore, note that an improvement is already made by using the upscaling approach only (orange line Figure 5B). However, in that case, only the response to the seasonal variation is captured. The response to monsoons (timescale of $\approx$20 days) is captured by the downscaling approach (purple). The relative contribution of each model improvement step indicates as well that the seasonal timescale (upscaling) is the most dominant (70%) in determining coastline evolution, followed by the monsoon response (downscaling, 23%). Figure 6B implies as well that the downscaling approach captures the smaller timescales (monsoons), while the larger timescales (seasonal variation) are captured by the upscaling approach.

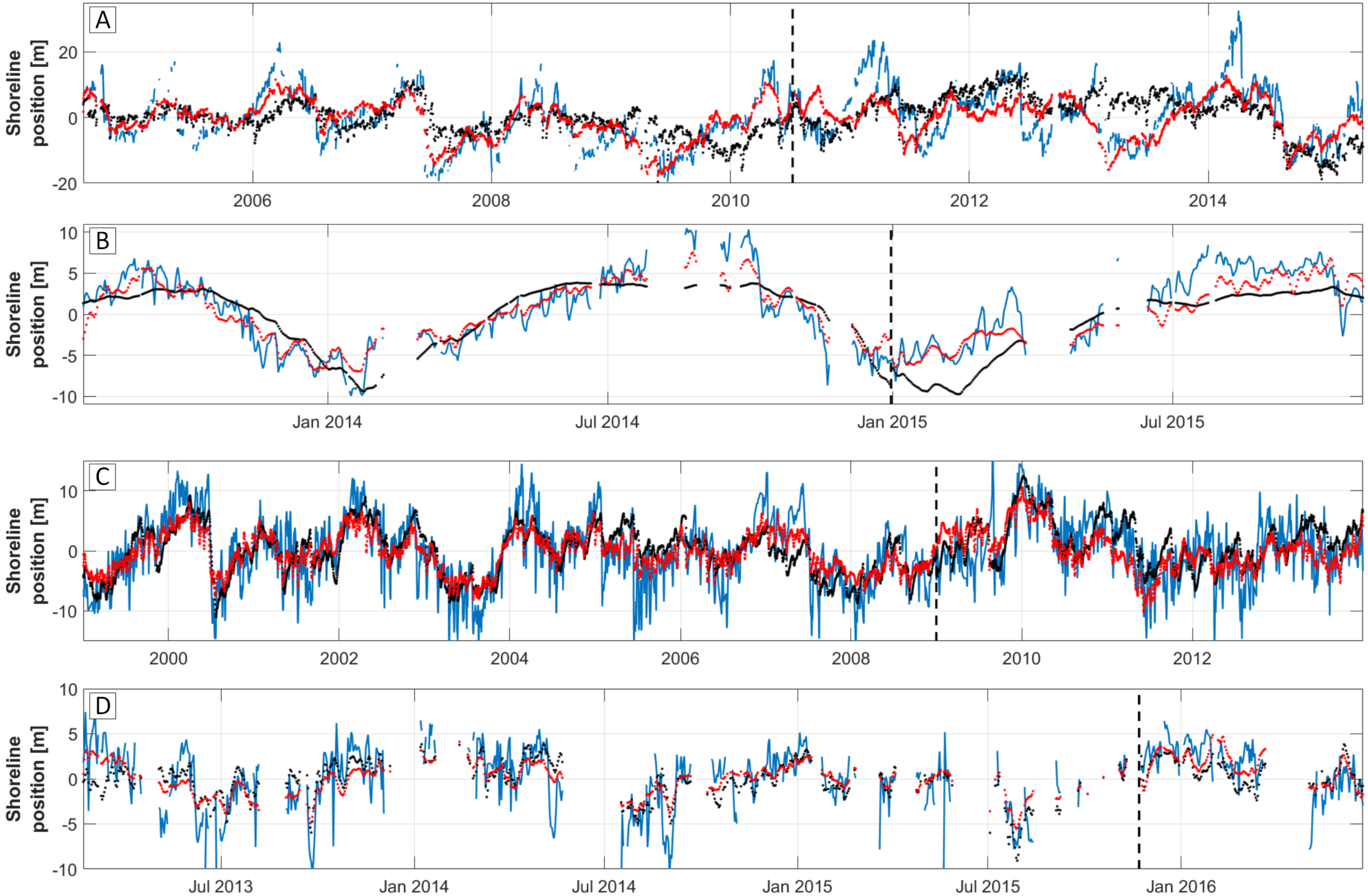

Figure 4. Model calibration and validation results using SF-ST (black) and SF-MT (red) for the dataset at Narrabeen (top), Nha Trang (second), Tairua (third) and Grand Popo (bottom). Note that the measured data is indicated in blue. The black dashed line indicates the discrimination between the calibration- and validation period.

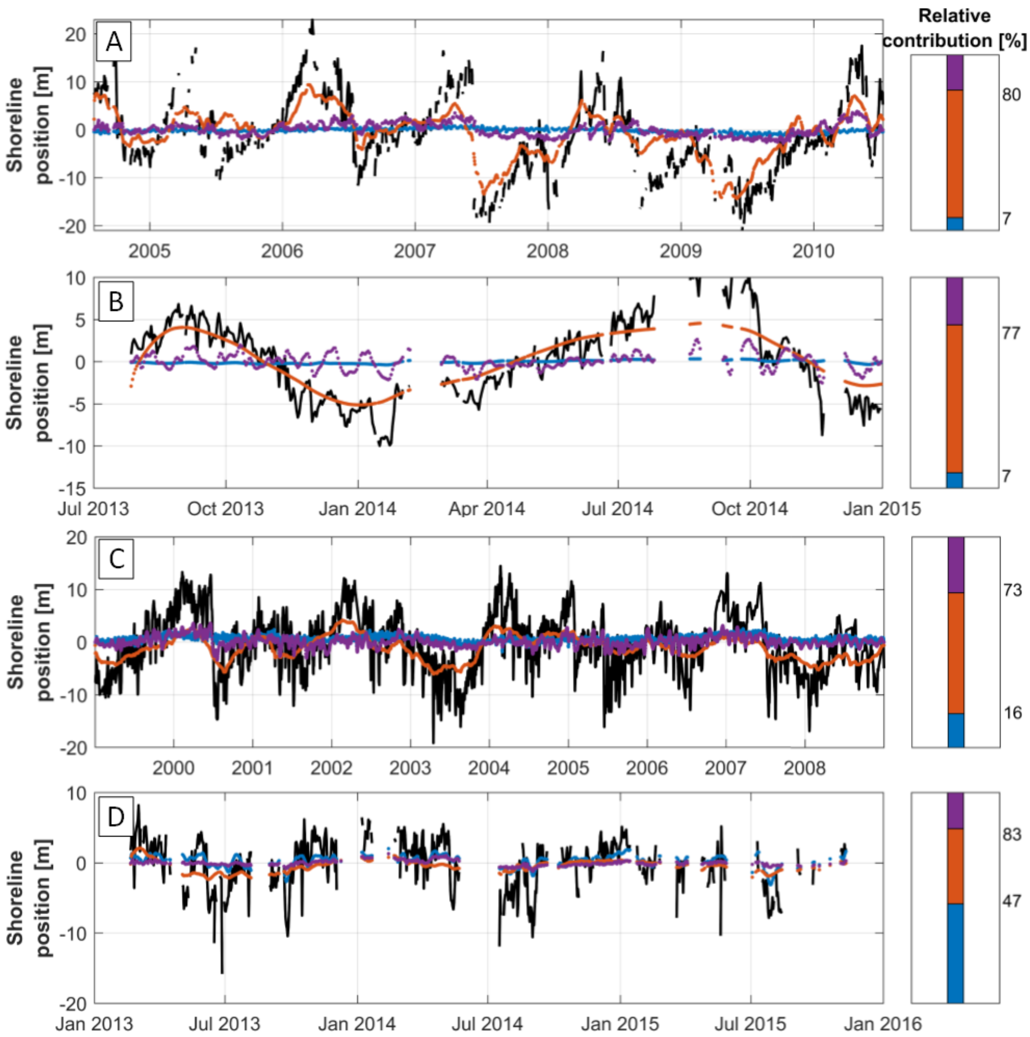

Figure 5. Contribution of each model improvement step over time (left panels) for the dataset at Narrabeen (top), Nha Trang (second), Tairua (third) and Grand Popo (bottom). Note that the measured data is indicated in black and the direct forcing-, upscaling- and downscaling approach are indicated in blue, orange and purple, respectively. Right: the corresponding relative contribution of the three model improvement steps.

From Figure 4C it becomes clear that the SF-ST (black, $\phi = 150$ days and $c = 1.03 * 10^{-7}$ $(m/s)/(W/m)^{0.5}$) and SF-MT (red) model both capture shoreline change well for the dataset at Tairua and at first sight model differences are less pronounced than for the dataset at Narrabeen and Tairua. The NMS error indicates that there are differences: 0.51 for SF-ST and 0.36 for SF-MT. However, they both correspond to a 'good' rating, although the error is considerably lower for SF-MT. This difference is also emphasized by the BSS of 0.3, indicating that the SF-MT is a 'good' improvement compared to SF-ST. The better model capability of SF-MT to capture shoreline change is emphasized as well in Figure 6C: both the standard deviation and the correlation for storm to monthly dominant timescales are higher for SF-MT. Those figures show as well that for the dominant seasonal to inter-annual timescales shoreline change is captured well by both models. However, there are certain moments in time where the SF-MT model outperforms SF-ST. This occurs for example at the end of 2006/beginning of 2007, where the accretion period is not well captured by SF-ST (Figure 4C). From Figure 5C and Figure 6C

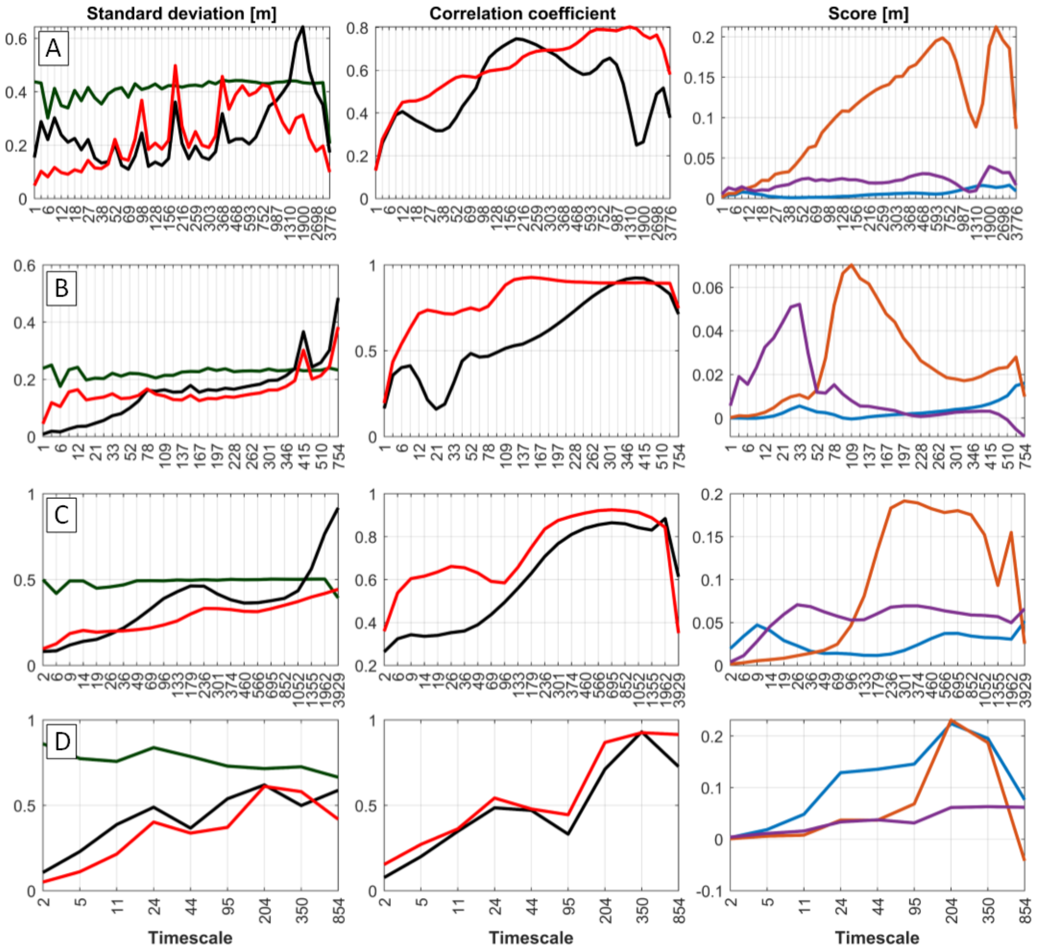

Figure 6. Standard deviation of the shoreline signals per timescale-cluster (left) for the data (green), SF-ST (black) and SF-MT (red), considering the dataset at Narrabeen (top), Nha Trang (second), Tairua (third) and Grand Popo (bottom). The second column indicates the correlation coefficient between the model result and data for SF-ST (black) and SF-MT (red) for every timescale-cluster and dataset. The third column shows a modelling score per timescale-cluster and model improvement step. The score consists of the correlation coefficient (data-model result) multiplied by the standard deviation (of the model result) at every timescale-cluster and for every model improvement step. The blue-, orange- and purple lines represent the direct forcing-upscaling and downscaling approach, respectively.

becomes clear that the larger dominant seasonal to inter-annual timescales are modelled using the upscaling approach (orange, 57%), the smaller timescales are modelled using the downscaling (monthly timescale, purple, 27%) and direct forcing approach (storm/swell timescale, blue, 16%).

At Grand Popo the difference in capturing shoreline change between SF-ST (ϕ = 7 days and $c = 7.63 \quad * \quad 10^{-8}$ $(m/s)/(W/m)^{0.5}$) and the SF-MT model is minor (Figure 4D). The NMS error between the data and SF-ST model result is 0.62 (a 'fair' rating), while it is 0.52 (a 'good' rating) for SF-MT. The BSS is 0.18, which corresponds to a 'fair' model improvement. The small difference between the two model results arises from the fact that the most dominant seasonal timescale is captured moderately better using SF-MT. This is emphasized in Figure 6D, where the correlation and standard deviation is similar and/or higher for SF-MT for the seasonal timescale. The daily to monthly timescales are captured with similar skill, or perhaps better using SF-ST as in particular more variability is present at those timescales, while the correlation is more or less the same. Figure 5D and Figure 6D show that the seasonal timescale is modelled by the direct forcing (blue) and upscaling (orange) approach and the storm/swell to monthly timescales by the direct forcing approach as well. The direct forcing approach contributes most to capturing shoreline change (47%), while the upscaling approach is responsible for modelling 36% of the shoreline variability. Signals generated with the downscaling approach have little contribution to the total modelled shoreline change signal (17%). It can be that this is due to the storm-free wave climate, for which the response could normally be captured by the downscaling approach. Nevertheless, the swell timescale is predicted poorly, even though this is a dominant mode of shoreline response (Table 2).

4.2 Validation

During model validation wave data in combination with the calibrated free parameters found in Section 4.1 are used to predict shoreline evolution. However, measured shoreline data is still available and is used to compare with the shoreline predictions. For the validation phase, shoreline predictions are shown in Figure 4 as well.

The validation results at Narrabeen reveal that the result of SF-MT outperforms that of SF-ST, but differences are less pronounced as for the calibration phase (BSS of 0.26 or a 'good' rating, compared to 0.61 or an 'excellent' rating for the calibration phase). From the time-series in Figure 4A, it becomes clear that especially after 2013, the prediction of SF-MT is closer to the data than the prediction of SF-ST. The NMS error between the data and model prediction is 0.83 for the SF-ST model, which reduces to 0.61 for the SF-MT model. This corresponds to a 'poor' and 'fair' rating, respectively. The overall variability of the beach is better represented by the SF-MT model, which is emphasized by the correlation coefficient (0.45 compared to 0.62, for SF-ST and SF-MT, respectively).

The model validation phase at Nha Trang shows similar characteristics as for the calibration phase as the seasonal variation and the response to summer- and winter monsoons are well predicted by SF-MT, while the SF-ST model only partially captures the seasonal variation (Figure 4B). The NMS error for SF-ST and the SF-MT model is 0.63 and 0.26, which corresponds to a 'fair' and 'excellent' rating, respectively. The similar characteristics for the calibration and validation phase are also emphasized by the BSS, which is 0.61 for the validation phase while it was 0.62 for the calibration phase (i.e. an 'excellent' rating).

A comparison of the validation results for both models at Tairua (Figure 4C) shows that some improvement is made by implementing multiple timescales in SF-ST, especially during the last 2 to 3 years of the dataset (BSS of 0.18 or a 'fair' model improvement). Overall, the SF-MT model predicts shoreline change better than SF-ST, which results in a decrease in the NMS error of 18% and an increase in the correlation coefficient of 8% (Table 3). The rating of the NMS error for SF-ST and SF-MT is 'fair' and 'good', respectively.

For the validation phase at Grand Popo a considerable improvement is made, which results in a NMS error of 0.47 for the SF-MT model (a 'good' rating), compared to 0.65 for SF-ST (a 'fair' rating). Signals generated by the direct forcing and upscaling approach contribute most to the improvement as those signals that

Site	Indicator	Calibration			Validation		
		SF-ST	SF-MT	%	SF-ST	SF-MT	%
Narrabeen	R	0.52	0.85	63	0.45	0.62	38
	NMSE	0.71	0.29	-59	0.83	0.61	-27
	BSS	-	0.61	-	-	0.26	-
	ΔAIC	-	>1	-	-	<1	-
Nha Trang	R	0.83	0.94	13	0.86	0.89	3
	NMSE	0.31	0.13	-58	0.63	0.26	-59
	BSS	-	0.62	-	-	0.61	-
	ΔAIC	-	>1	-	-	<1	-
Tairua	R	0.70	0.85	21	0.60	0.65	8
	NMSE	0.51	0.36	-29	0.71	0.58	-18
	BSS	-	0.3	-	-	0.18	-
	ΔAIC	-	>1	-	-	<1	-
Grand Popo	R	0.62	0.73	18	0.47	0.60	28
	NMSE	0.62	0.52	-16	0.65	0.47	-28
	BSS	-	0.18	-	-	0.30	-
	ΔAIC	-	<1	-	-	<1	-

Table 3. Model skill during the calibration and validation phase, for the SF-ST and SF-MT model, at all four sites, using four model skill indicators.

make sure that the dominant seasonal variation is better captured (as observed in Section 4.1). The BSS is 0.30, which corresponds to a ‘good’ rating.

4.3 Overview model improvement

Table 3 presents the modelling skill of the SF-ST and SF-MT model, per study site, for the calibration and validation phase by using four different model skill indicators: the correlation coefficient, the NMS error, the BSS score and ΔAIC.

For the dataset at Narrabeen the model improvement during the calibration phase is considerable (BSS of 0.61 or an ‘excellent’ rating), while it is less pronounced for the validation phase (BSS of 0.26 or a ‘good’ rating). The correlation coefficient is substantially larger for SF-MT during the calibration as well as for the validation phase (63% and 28%, respectively). The ΔAIC score (difference in AIC score between SF-ST and SF-MT) is larger than 1 for the calibration phase and smaller than 1 for the validation phase. This indicates that a considerable model improvement is acquired during the calibration phase. Conversely, during the validation phase the SF-ST model is preferred according to this score, due to the trade-off between the model’s simplicity and goodness of fit. The ΔAIC score indicates that for the SF-MT model the number of calibration parameters (i.e. decreased model simplicity), which is penalized for by the AIC score (Equation B3), is too large compared to the goodness of fit (relative to SF-ST).

Considering the Nha Trang dataset, model improvement is large for the calibration phase as well as for the validation phase, as the NMS error rating increases from a 'good' rating to an 'excellent' rating and a 'fair' to 'excellent' rating for the calibration and validation phase, respectively. The correlation coefficient is improved less considering the calibration and validation phase (13% and 3%, respectively) when comparing SF-MT to SF-ST. This is due the the fact that both models capture and correlate with the (most) dominant seasonal response. The BSS also indicates substantial model improvement during model calibration and validation, corresponding to an 'excellent' rating for both phases. The ΔAIC score is larger/smaller than 1 for the calibration/validation phase. This implicates that during the calibration phase the larger number of calibration parameters in the SF-MT model is justified by a considerably better model fit (relative to SF-ST), while this is not the case for the validation phase.

At Tairua, the NMS error is moderately decreased by using SF-MT compared to SF-ST during the calibration and validation phase (29% and 18%, respectively). The same is true for the correlation coefficient, with increases of 21% and 8%, while the BSS corresponds to a 'good' and 'fair' rating for the calibration and validation phase, respectively. The moderately increased performance of SF-MT over SF-ST can partly be explained by the fact that both models capture the most dominant seasonal to inter-annual response, while the SF-MT model better captures shoreline change on the dominant monthly timescale. The ΔAIC score is larger than 1 for the calibration phase and smaller than 1 for the validation phase. This indicates that a considerable model improvement is acquired during the calibration phase, while during the validation phase the SF-ST model is preferred due to the model's simplicity compared to the relative goodness of fit.

For the calibration phase at Grand Popo, model improvement is less impressive compared to other sites as the NMS error reduces from 0.62 (a 'fair' rating) to 0.52 (a 'good' rating) for SF-ST and SF-MT, respectively. For the validation phase the improvement is more pronounced (28%). For both modelling phases the correlation coefficient is increased as well, when comparing SF-ST to SF-MT (18% and 28% for the calibration and validation phase, respectively). The BSS for the calibration phase yields a 'fair' rating. The BSS for the validation phase yields a 'good' rating, which indicates that the model result of SF-MT is considerably closer to the measured data than the baseline prediction (i.e. the SF-ST model). Note that all scores are larger for the validation phase than for the calibration phase, which is probably due to the fact that the validation time-frame is rather short (Table 1). The ΔAIC score is smaller than 1 for both modelling phases, indicating that SF-ST is the preferred model because of the model's simplicity relative to the goodness of fit.

5 Discussion

This work was motivated by the fact that single memory decay models fail to reproduce shoreline evolution at equatorial West-African and tropical Vietnamese sites over timescales of 2-3 years, where multiple forcing timescales are present, such as seasonal and monsoon forcing. In this paper, we focused on a single memory decay hybrid model that predicts temporal changes of the shoreline location due to varying wave conditions. Although there are hybrid models that account for shoreline change due to for example cross-shore and longshore processes, sea level rise and include the beach-dune system (e.g., Antolínez et al., 2019; Vitousek et al., 2017; Robinet et al., 2018, 2020), here the focus was on shoreline changes due to cross-shore processes only. The hybrid model used here as a base is the ShoreFor model (SF-ST; Shoreline Forecast - Single Timescale - see description in Appendix A), by Davidson et al. (2013). This model uses a holistic understanding of how a beach responds to several high-intensity forcing event characteristics (duration, intensity, clustering and recovery, see Appendix A). The key model free parameter is the memory decay factor (ϕ), which indicates the single most dominant response time of cross-shore sediment exchange. However, due to this single memory decay factor, model skill deteriorates considerably if multiple dominant forcing and beach response timescales are present (Vitousek et al., 2017; Almar et al., 2017; Splinter et al., 2017). Recent work by Splinter et al. (2017) and Ibaceta et al. (2020) also showed that timescales of beach change and forcing may be temporally dependent, with beaches undergoing rapid adjustment to the changes in the dominant wave forcing over time and where single memory decay models can fail to capture the observed shoreline signal.

Besides the literature mentioned in Section 2, the temporal spectra (Section 3.1 and Figure C1) reveal the presence of multiple dominant timescales. These spectra can be considered before model application and can be used to determine if the SF-MT model is more favorable to use with respect to SF-ST (considering model complexity): multiple dominant forcing timescales lead to a substantial improvement (e.g. Narrabeen and Nha Trang, BSS of 0.61 and 0.62, respectively), while if a single timescale is present a less substantial improvement can be expected (Tairua, BSS of 0.30). At Grand Popo model improvement is also less substantial (BSS of 0.18), while there are multiple dominant forcing timescales present. However, it should also be mentioned that in terms of forcing, this site is very unique (other than multiple dominant forcing components): see for example Ondoa et al. (2020), in which they reveal that intra-seasonal sea level variations impact the beach profile, which is a process that is not accounted for in the model. Moreover, at Narrabeen, Nha Trang and Tairua, the ΔAIC score is larger than 1 for the calibration phase, indicating a considerable model improvement is acquired when accounting for model skill and complexity. However, for the validation phase the ΔAIC score is smaller than 1. In case of a low/negative ΔAIC score and a limited number of observed dominant timescales, a reduced number of bins can also be tested to increase the ΔAIC score. Nevertheless, SF-MT currently handles a large number of 'blind' bins by giving low/no weight to timescale-clusters where low variability is observed to have an unbiased result regarding timescale interactions (rather than hardwire on dominant timescales before model application). The multi-timescale model outperforms SF-ST at sites where short-term (2-3 years) and long-term (10-14 years) data is available. Interestingly, for longer period simulations, climate variability induces changes in wave regimes at all scales, storminess of storm tracks in mid-latitudes, tropical cyclones, but also monsoons and seasonal to inter-annual average conditions (Vitousek et al., 2017; Melet et al., 2020). Moreover, as a variable climate is expected, multiple timescales of shoreline adjustment to forcing likely exist almost everywhere. In that context, the humble simplified approach developed in SF-MT can be an attractive way to capture shoreline change to climate modes, climate change and their timescale-interactions.

Apart from a considerable increase in model prediction skill (Table 3), compared to SF-ST, the SF-MT model also gains insight in how a beach responds to the considered wave-forcing on multiple scales. The contribution of each model improvement step to shoreline evolution (Figure 5 & 6), illustrates for example that at all sites extreme forcing events have a considerable and persistent shoreline impact (i.e. upscaling approach). It showed that these forcing events are responsible for 36 to 73% of the variability of shoreline evolution. At Narrabeen, Nha Trang and Tairua, long term shoreline trends affect short term forcing event impacts (i.e. downscaling approach). These affected short term forcing event impacts are responsible for 17 to 27% of the variability of shoreline evolution. At Grand Popo those mechanisms are not the main driver of shoreline variability. There the wave forcing drives, for a large part, shoreline change on corresponding timescale-clusters (i.e. direct forcing approach), which could be one of the causes why the model result of SF-MT it is closest to the SF-ST model performance. Moreover, the distribution of shoreline variability over the different modelling approaches and timescale-clusters in SF-MT (last column in Figure 6), showed that the upscaling approach is responsible for capturing shoreline change on the largest timescales in the dataset, as this approach is modelling the persistent effect of short high-intensity wave forcing events on larger timescale shoreline response. Conversely, the modelled shorelines generated with the downscaling approach correspond better to shoreline data on smaller timescales, as this approach is modelling the effect of the larger timescales in shoreline variation on the efficiency which with smaller timescale wave-forcing events induce cross-shore sediment transport. The direct forcing approach does not account for particular shoreline response timescales as it seems to be dataset dependent.

The SF-MT model generates multiple individual signals, in which each signal (i.e. timescale-cluster) has a unique timescale relation between the wave forcing and shoreline signal. A certain selection of all these generated signals make up the total shoreline signal (Section 3.3). To visualize these unique timescale relations of all chosen modelled signals, a grid of timescale interactions is presented (Figure 7). In those grids the percentage to the total shoreline signal per individual modelled signal (i.e. timescale-cluster) is plotted, revealing the most important timescale interactions per dataset. The axes can be used to check which timescales are considered and the diagonal, upper left corner and lower right corner correspond to signals generated with the direct forcing, upscaling, and downscaling approach, respectively. Figure 7 presents the timescale interactions at Narrabeen (top), Nha Trang (middle) and Tairua (bottom). Due to the limited number of timescale-bins, the grid of timescale interactions will not be shown for the dataset at Grand Popo.

The interactions between timescales shown in Figure 7A show that at Narrabeen the short-term high-intensity forcing events with a timescale of approximately 1 to 6 days have a large and persistent impact on the large timescale shoreline variation (quasi-seasonal). Moreover, shoreline variability on inter-annual timescales is driven by variations in the wave climate with a similar timescale, but it is sensitive to whether the coastline is eroded or accreted on a mildly larger timescale of approximately 860-1134 days (i.e. downscaling approach). This means that the impact to inter-annual forcing events is dependent on whether that coastline is eroded or accreted on a similar to larger timescale.

In contrast, Figure 7B shows that at Nha Trang small(er) timescales in the wave forcing (especially those with a timescale of 123-197 days) have a persistent and considerable effect on coastline evolution, and which is together with the persistent effect of monsoons the cause of the seasonal variability (i.e. upscaling). Furthermore, as indicated by the time-series in Figure 5B, shoreline response to both summer and winter monsoons is affected by longer term shoreline variations (i.e. downscaling). This means that the response to these monsoons is not equal throughout the year. Beach response to monsoons (with a timescale of approximately 10-30 days) is larger when the shoreline is already accreted on a larger timescale (3 months or 1.5 year, see Figure 7B). This supports the fact that due to an overall accreted beach state, the offshore sand supply is close to the shoreline, which yields a high sediment transport efficiency and faster response to monsoons. Conversely, when the coastline is already eroded on a larger timescale, the monsoon response is relatively smaller: a large spatial separation between the shoreline and the offshore sediment source yields an inefficient transfer of sediment between the offshore region and beach face, causing a lower response rate. Hence, at Nha Trang the beach response to winter monsoons is relatively smaller than the response to summer monsoons.

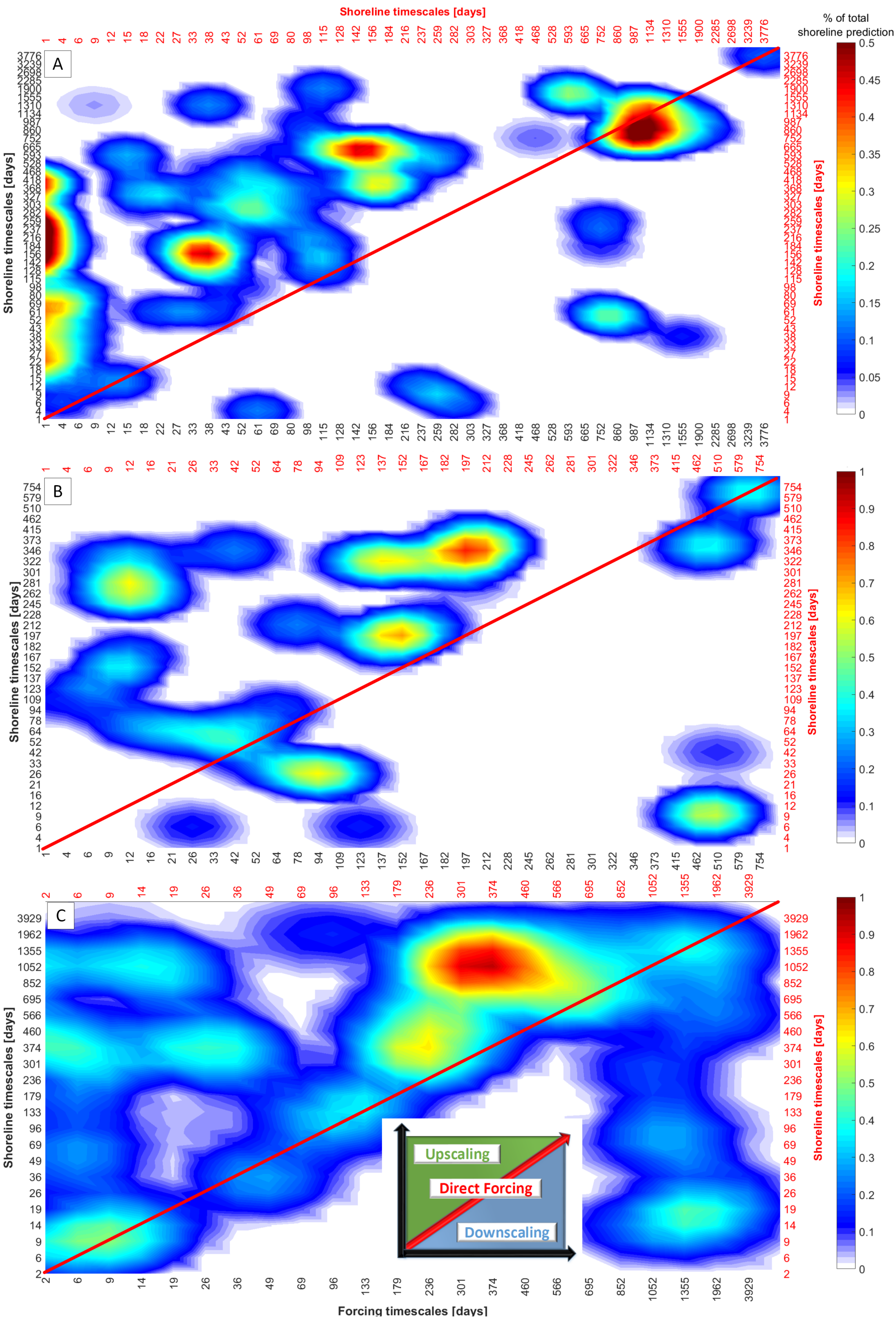

Figure 7. Timescale interactions at Narrabeen (top), Nha Trang (middle) and Tairua (bottom) and the corresponding legend (bottom). The diagonal represents signals modelled with the direct forcing approach where the black axes (from x to y) can be used to check which timescales are involved. For the upscaling approach (all patches in the upper left corner) the black axes can be used as well. The lower right corner of the grid represents signals generated with the downscaling approach. For those patches the red axes need to be used (from x to y). The colour indicates the percentage of those signals to the total modelled shoreline. A smooth function is used to visually highlight the most dominant timescale interactions.

Figure 7C visualizes the timescale interactions at Tairua. It shows that the wave forcing with an annual timescale has a large and persistent impact on the inter-annual shoreline response (852-1355 days). Moreover, shoreline response on the smallest (storm/swell) timescales (6-9 days) is driven by wave forcing events on a similar timescale (i.e. direct forcing). Furthermore, the inter-annual shoreline change has an influence on how the beach responds to the short timescale wave forcing events with a timescale of approximately 9 to 26 days.

6 Conclusions

In this study, a new approach is presented to allow for multiple wave forcing- and beach response timescales within the single timescale- equilibrium shoreline prediction model ShoreFor (SF-ST; Shoreline Forecast - Single Timescale). While SF-ST was capable of accurately predicting shoreline change only on the single most dominant beach response timescale, multiple dominant timescales can determine shoreline evolution. The multi-timescale implementation (SF-MT; Shoreline Forecast - Multiple Timescales) is governed by filtering and identifying all of the wave forcing and shoreline response timescales. Subsequently, timescales in the wave forcing and shoreline signals are linked through three new terms in the model which are direct forcing, upscaling and downscaling. In the direct forcing term, the shoreline is forced by waves on the corresponding timescales (e.g. a beach erodes and recovers to an individual storm). The upscaling term accounts for the persistent effect of short(er) forcing timescales on longer shoreline response timescales (e.g. seasonal persistence of summer- and winter monsoons). This is modelled using the envelope of the filtered wave signals, which provides the timescale link. The downscaling approach governs the effect of long(er) timescales of shoreline evolution on shoreline response to short(er) wave forcing timescales (e.g. storm impact during accreting or eroding trends). The effect is modelled by introducing a time-dependent response factor from a longer timescale shoreline evolution signal. The multi-timescale model showed considerable improvement compared to SF-ST at the four contrasted sites used in this study. This combined approach leads to several interests when considering interplay between climate modes and storminess under climate change when forecasting future shoreline evolution.

Acknowledgments

Rob Schepper would like to thank LEGOS, the Delft University of Technology and IMDC for providing the opportunity to write this paper and secondly, he is grateful to LEGOS, the University of Plymouth, the Water Research Laboratory of the University of New South Wales and the University of Auckland for providing the datasets used in this study. He is also grateful to Dr. Caroline Katsman of the Delft University of Technology for her contribution to this paper. Dr. Erwin Bergsma was funded through a post-doctoral fellowship of the French National Space Agency (CNES - Centre National d'Etudes Spatiales). The data at Nha Trang and Grand Popo can be accessed through the following link: https://doi.org/10.5281/zenodo.3669126. The data at Tairua can be accessed through: https://coastalhub.science/data.

Appendix A ShoreFor (SF-ST), the original single timescale model

ShoreFor (SF-ST; Shoreline Forecast - Single Timescale) (Davidson et al., 2013) is an equilibrium shoreline prediction model, which employs the concept of (dis-)equilibrium of shoreline location following Wright et al. (1985), to predict shoreline change. The SF-ST model takes the following form to estimate temporal shoreline change (Splinter et al., 2014; Splinter et al., 2017):

$$\frac{dx_s}{dt} = c(F(\phi)^+ + rF(\phi)^-) + b \tag{A1}$$

Wherein dx_s/dt is the rate of shoreline change, t the time, c a response rate parameter, ϕ the memory decay factor, r the erosion/accretion ratio, b the linear trend term and F the wave forcing term. The forcing term is divided into an accretionary (F^+) and erosional component (F^-), because the accretionary and erosion responses are governed by different processes.

The SF-ST model describes the wave forcing using the dimensionless fall velocity (Ω, see e.g. Gourlay (1968); Dean (1973)):

$$\Omega = \frac{H_s}{w_s T_p} \tag{A2}$$

wherein H_s and T_p being respectively the deep-water significant wave height and peak period and w_s the sediment fall velocity.

Both forcing terms in equation A1 are determined by:

$$F = P^{0.5}\frac{\Delta\Omega}{\sigma_{\Delta\Omega}} \tag{A3}$$

Where P is the wave power ($\propto \quad H_s^2 T_p$ in deep water), $\Delta\Omega$ the disequilibrium of dimensionless fall velocity ($\Omega_{eq} - \Omega$) with Ω_{eq} being a dynamic equilibrium term, Ω the instantaneous dimensionless fall velocity and $\sigma_{\Delta\Omega}$ the standard deviation of the disequilibrium. The disequilibrium term ($\Delta\Omega$) determines whether the coastline is accreting or eroding (plus and minus, respectively (Davidson et al., 2013)) and dividing by the standard deviation of the disequilibrium makes sure that only the wave energy flux (P) and response rate parameter (c) determine the rate of shoreline change, rather than the magnitude of disequilibrium. The dynamic equilibrium term accounts for the fact that future shoreline positions can be strongly dependent on past hydrodynamic conditions (Davidson et al., 2013) and can be, following Wright et al. (1985), defined as follows:

$$\Omega_{eq} = \frac{\sum_{i=1}^{2\phi} \Omega_i 10^{\frac{-i}{\phi}}}{\sum_{i=1}^{2\phi} 10^{\frac{-i}{\phi}}} \tag{A4}$$

in which i is the number of days in the wave forcing time-series prior to the day of observation, Ω_i the dimensionless fall velocity and ϕ the memory decay factor. A large memory decay factor (>>100 days) generates a large timescale shoreline response (e.g. a seasonal variation), while a small decay factor (<100 days) produces a shoreline prediction where smaller (storm) timescales are dominant (Splinter et al., 2014).

The linear trend term in equation A1 captures shoreline changes that do not result from wave driven- cross-shore sediment transport processes (e.g. gradients in long-shore sediment transport). Furthermore, note that c and ϕ are site-specific calibration parameters, while r is not a model free parameter. In absence of the erosion parameter (r), a strong erosive trend would be predicted as negative disequilibrium conditions (e.g. storms) often have a higher associated wave power

(Stokes et al., 2015). This erosion ratio parameter is based on the assumption that the detrended erosion and accretion forcing are assumed equal: it maintains a long-term shoreline equilibrium if no trend in the wave forcing data is present.

The SF-ST model seeks the best relation between the raw wave forcing- and raw shoreline position data through the fitting of several calibration parameters (c & ϕ) using the knowledge of how the beach responds to incoming wave forcing. For example, a beach in equilibrium with the current and antecedent (calm) forcing conditions will try to adapt to a new equilibrium if wave conditions change, like in the case of a high-intensity forcing event (e.g. a storm) impacting the coastline. During such event, the beach will erode and the shoreline moves landward. The new established shoreline is then more in equilibrium with the prevailing forcing. However, several characteristics of the high-intensity forcing event play a role in how the (modelled) shoreline position responds to the considered wave forcing. The first aspect is the forcing duration: only if the duration is long enough (i.e. stationary conditions), a new equilibrium is established. Secondly, the intensity of the wave forcing determines how far the beach retreats. Thirdly, in case of multiple high-intensity forcing events, the sequence of these forcing events (e.g. a storm cluster) determines to a large extent the shoreline change. Here, the first wave forcing event in the cluster is more effective in eroding the shoreline, because the disequilibrium is the largest (Yates et al., 2009). A prerequisite, for the sequencing to be important, is that the beach has no time to fully recover in between the high-intensity forcing events that make up the cluster (Angnuureng et al., 2017; Karunarathna et al., 2014). To what extent a beach recovers from the antecedent high-intensity forcing conditions mainly depends on the characteristics of the post-storm hydrodynamic conditions relative to the antecedent conditions (Morton et al., 1994). The SF-ST model is only applicable on locations where wave driven-, cross-shore processes dominate sediment transport and where anthropological influences are minimal (Davidson et al., 2013). SF-ST was originally established using data in micro-tidal environments (see Davidson et al. (2013)), but the subsequent model of Splinter et al. (2014) was established covering a wide range of tidal ranges. Moreover, Dodet et al. (2019) showed that the model yields significant skill in reproducing post-storm recovery in a macro-tidal environment as well. However, here model training sites with a limited tidal range are used, to minimize the influence of the tide on the shoreline location.

Appendix B Model skill assessment

To evaluate model prediction skill, the total shoreline prediction for both the calibration- and validation phase is compared to the corresponding measured shoreline location data. The first model skill indicator that is used is the correlation coefficient. The correlation coefficient indicates the strength of the relationship between the modelled- and measured shoreline data. The other three model skill indicators are: 1) the normalized mean square error (NMSE) between the modelled and measured data and 2) the Brier Skill Score (BSS), which can take measurement errors into account and 3) the ΔAIC value, which accounts for model complexity. The NMSE (Miller & Dean, 2004; Splinter et al., 2013) compares the error variance to the observed variance and is chosen to allow for easier skill comparison between each site, compared to the Root Mean Squared Error (RMSE). The NMSE can be written down as:

$$NMSE = \frac{\sum(x_m - x)^2}{\sum x_m^2} \tag{B1}$$

In which x_m is the measured shoreline and x the modelled shoreline. A NMSE of 0-0.3, 0.3-0.6, 0.6-0.8, 0.8-1.0 is labeled as 'excellent', 'good', 'fair' and 'poor', respectively (Splinter et al., 2014).

The Brier Skill Score (van Rijn et al., 2003; Sutherland et al., 2004) compares the performance of two models to the observed shoreline location and has the following form (adopted after Bosboom and Reniers (2017)):

$$BSS = \frac{\langle (x_b - x_m)^2 \rangle - \langle (x - x_m)^2 \rangle}{\langle (x_b - x_m)^2 \rangle - 2\delta^2} \tag{B2}$$

Wherein x_m is the measured shoreline, x the modelled shoreline, δ the measurement error and x_b the baseline model. In this paper, SF-ST will be used as a baseline model. The triangle brackets indicate the mean. Positive BSS indicate a significant model improvement relative to this baseline model where values between 0-0.1, 0.1-0.2, 0.2-0.5 and 0.5-1.0 are labeled as 'poor', 'fair', 'good' and 'excellent', respectively. Note that the formulation of the BSS has been adopted after Bosboom and Reniers (2017). They advise the use of the skill formulation according to Sutherland et al. (2004) in combination with a classification that is not adjusted for measurement error as is used here. A constant measurement error of 0.5 meter is used, as for all sites the shoreline location time-series are extracted from video-images.

By using SF-MT, the total predicted shoreline signal consists of multiple signals with different timescales. For each individual modelled signal using the direct forcing- and upscaling approach (Equations 1 and 2), two calibration parameters are present: the memory decay factor (ϕ) and the response factor (c). For the downscaling approach (Equation 3) only one calibration parameter is present: the memory decay factor. Therefore, the fourth model skill indicator that will be used is the Akaike's information criterion (AIC) (Akaike, 1974) as it is specifically designed to compare models with a different number of calibration parameters (m):

$$AIC = n * (log(2\pi) + 1) + n * log(\sigma^2) + 2m \tag{B3}$$

In which n is the total number of samples and σ^2 the variance of the model or baseline residuals. Hence, it deals with the trade-off between the goodness of fit and model simplicity. If the difference between the baseline and model AIC (ΔAIC) exceeds 1.0, a considerable model improvement is acquired (Davidson et al., 2013). In this study SF-ST will be used as a baseline model.

Appendix C Temporal spectra of the wave- and shoreline data

This Appendix shows how the dominant timescales in the shoreline- and wave forcing time-series were determined (Table 2). Dominant timescales were obtained by determining local peaks (using a peak analysis tool) in the temporal spectra. The temporal spectra for the shoreline position, wave height and wave period are shown in Figure C1 for each dataset. The most dominant timescale per spectrum is indicated with a red circle, while other dominant timescales can be identified by other local peaks in the temporal spectra.

References

Aagaard, T., Kroon, A., Andersen, S., Sørensen, R. M., Quartel, S., & Vinther, N. (2005). Intertidal beach change during storm conditions; egmond, the netherlands. *Marine Geology*, *218*, 65-80.

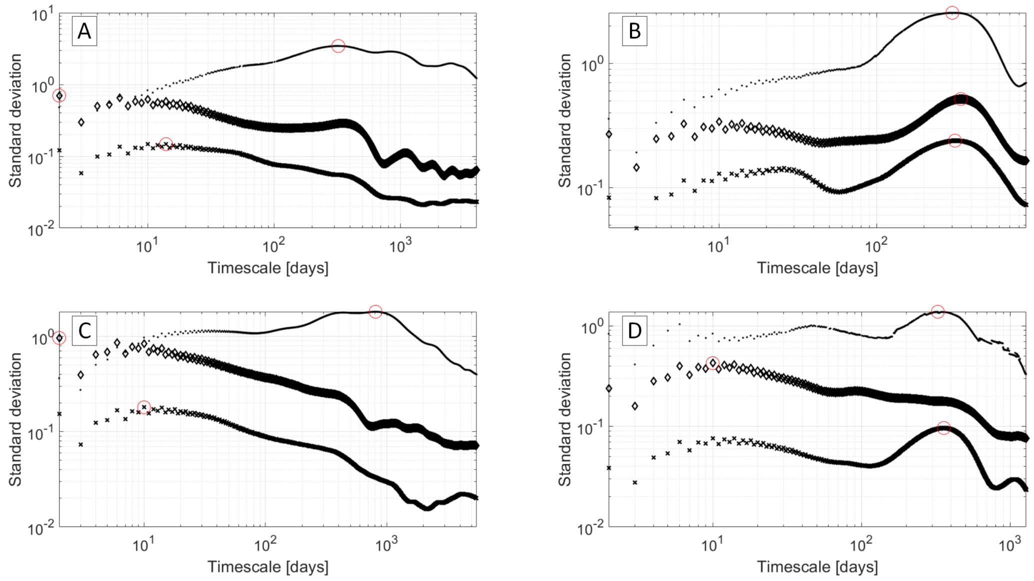

Figure C1. Temporal spectra of the shoreline position (dotted), wave height (crosses) and wave period (diamonds), for all datasets. The red circle indicates the most dominant timescale. The top left, top right, bottom left and bottom right panel is corresponding to the dataset at Narrabeen, Nha Trang, Tairua and Grand Popo, respectively.

Akaike, H. (1974). A new look at the statistical model identification. *IEEE Transactions on Automatic Control*, *19*(6), 716-723.

Almar, R., Kestenare, E., Reyns, J., Jouanno, J., Anthony, E., Laibi, R., … Ranasinghe, R. (2015, November). Response of the bight of benin (gulf of guinea, west africa) coastline to anthropogenic and natural forcing, part1: Wave climate variability and impacts on the longshore sediment transport. *Continental Shelf Research*, *110*, 48–59. Retrieved from `https://doi.org/10.1016/j.csr.2015.09.020` doi: 10.1016/j.csr.2015.09.020

Almar, R., Marchesiello, P., Almeida, L. P., Thuan, D. H., Tanaka, H., & Viet, N. T. (2017). Shoreline response to a sequence of typhoon and monsoon events. *Water*, *9*(52).

Anderson, T. R., Frazer, L. N., & Fletcher, C. H. (2010, April). Transient and persistent shoreline change from a storm. *Geophysical Research Letters*, *37*(8). Retrieved from `https://doi.org/10.1029/2009gl042252` doi: 10.1029/2009gl042252

Angnuureng, D. B., Almar, R., Senechal, N., Castelle, B., Addo, K. A., Marieu, V., & Ranasinghe, R. (2017). Shoreline resilience to individual storms and storm clusters on a meso-macrotidal barred beach. *Geomorphology*, *290*, 265 - 276. Retrieved from `http://www.sciencedirect.com/science/article/pii/S0169555X17301496` doi: https://doi.org/10.1016/j.geomorph.2017.04.007

Anthony, E., Almar, R., Besset, M., Reyns, J., Laibi, R., Ranasinghe, R., … Vacchi, M. (2019, February). Response of the bight of benin (gulf of guinea, west africa) coastline to anthropogenic and natural forcing, part 2: Sources and patterns of sediment supply, sediment cells, and recent shoreline change. *Continental Shelf Research*, *173*, 93–103. Retrieved from `https://doi.org/10.1016/j.csr.2018.12.006` doi: 10.1016/j.csr.2018.12.006

Antolínez, J. A. A., Méndez, F. J., Anderson, D., Ruggiero, P., & Kaminsky, G. M. (2019, June). Predicting climate-driven coastlines with a simple and efficient multiscale model. *Journal of Geophysical Research: Earth Surface*, *124* (6), 1596–1624. Retrieved from `https://doi.org/10.1029/2018jf004790` doi: 10.1029/2018jf004790

Bergsma, E., & Almar, R. (2020, June). Coastal coverage of ESA' sentinel 2 mission. *Advances in Space Research*, *65* (11), 2636–2644. Retrieved from `https://doi.org/10.1016/j.asr.2020.03.001` doi: 10.1016/j.asr.2020.03.001

Bergsma, E., Conley, D., Davidson, M., OHare, T., & Almar, R. (2019, March). Storm event to seasonal evolution of nearshore bathymetry derived from shore-based video imagery. *Remote Sensing*, *11* (5), 519. Retrieved from `https://doi.org/10.3390/rs11050519` doi: 10.3390/rs11050519

Blossier, B., Bryan, K. R., Daly, C. J., & Winter, C. (2017, October). Shore and bar cross-shore migration, rotation, and breathing processes at an embayed beach. *Journal of Geophysical Research: Earth Surface*, *122* (10), 1745–1770. Retrieved from `https://doi.org/10.1002/2017jf004227` doi: 10.1002/2017jf004227

Bosboom, J., & Reniers, A. (2017). The deceptive simplicity of the brier skill score. *Handbook of Coastal and Ocean Engineering: Expanded Edition*, *2-2*, 1639-1663.

Bradshaw, B., Healy, T. R., Dell, P. M., & Bolstad, W. (1991). Inner shelf dynamics on a storm-dominated coast, east coromandel, new zealand. *Journal of Coastal Research*, *7* (1), 11-30. Retrieved from `https://www.jstor.org/stable/4297802`

Callaghan, D. P., Ranasinghe, R., & Roelvink, D. (2013). Probabilistic estimation of storm erosion using analytical, semi-empirical, and process based storm erosion models. *Coastal Engineering*, *82*, 64-75.

Davidson, M. A., Splinter, K. D., & Turner, I. L. (2013). A simple equilibrium model for predicting shoreline change. *Coastal Engineering*, *73* (52), 191-202.

Davidson, M. A., Splinter, K. D., Turner, I. L., & Harley, M. D. (2017). Annual prediction of shoreline erosion and subsequent recovery. *Coastal Engineering*.

Dean, R. G. (1973). Heuristic models of sand transport in the surfzone. *Proc. of the 1st Australian Conference on Coastal Engineering, Engineering Dynamics in The Surf Zone, Sydney, Australia*, 209-214.

Dodet, G., Castelle, B., Masselink, G., Scott, T., Davidson, M., Floc'h, F., ... Suanez, S. (2019). Beach recovery from extreme storm activity during the 2013-14 winter along the atlantic coast of europe. *Earth Surface Processes and Landforms*, *44*, 393-401.

Frazer, L. N., Anderson, T. R., & Fletcher, C. H. (2009, October). Modeling storms improves estimates of long-term shoreline change. *Geophysical Research Letters*, *36* (20). Retrieved from `https://doi.org/10.1029/2009gl040061` doi: 10.1029/2009gl040061

Goldstein, E. B., Coco, G., & Plant, N. G. (2019, July). A review of machine learning applications to coastal sediment transport and morphodynamics. *Earth-Science Reviews*, *194*, 97–108. Retrieved from `https://doi.org/10.1016/j.earscirev.2019.04.022` doi: 10.1016/j.earscirev.2019.04.022

Gourlay, M. R. (1968). Beach and dune erosion tests. *Delft Hydraulics Laboratory Report m935/m936, Delft, The Netherlands*.

Harley, M. D., Turner, I., Short, A., & Ranasinghe, R. (2011). A reevaluation of coastal embayment rotation: the dominance of cross-shore versus alongshore sediment transport processes in se australia. *Journal Of Geophysical Research*, *116* (16).

Harley, M. D., Turner, I. L., Short, A. D., & Ranasinghe, R. (2009). Interannual variability and controls of the sydney wave climate. *International Journal of Climatology*, n/a–n/a. Retrieved from `https://doi.org/10.1002/joc.1962` doi: 10.1002/joc.1962

Holman, R. A., & Stanley, J. (2007). The history and technical capabilities of argus.

Coastal Engineering, *54* (6-7), 477-491.
Ibaceta, R., Splinter, K. D., Harley, M. D., & Turner, I. L. (2020, November). Enhanced coastal shoreline modeling using an ensemble kalman filter to include nonstationarity in future wave climates. *Geophysical Research Letters*, *47* (22). Retrieved from `https://doi.org/10.1029/2020gl090724` doi: 10.1029/2020gl090724
Jackson, N., Nordstrom, K., Eliot, I., & Masselink, G. (2002). "low energy" sandy beaches in marine and estuarine environments: A review. *Geomorphology*, *48*, 147-162.
Karunarathna, H., Pender, D., Ranasinghe, R., Short, A. D., & Reeve, D. E. (2014). The effects of storm clustering on beach profile variability. *Marine Geology*, *348*, 103 - 112. Retrieved from `http://www.sciencedirect.com/science/article/pii/S0025322713002624` doi: https://doi.org/10.1016/j.margeo.2013.12.007
Larson, M., & Kraus, N. C. (1995). Prediction of cross-shore sediment transport at different spatial and temporal scales. *Marine Geology*, *126* (1-4), 111-127.
Lefebvre, J.-P., Almar, R., Viet, N. T., Thuan, D. H., Binh, L. T., Ibaceta, R., & Duc, N. V. (2014). Contribution of swash processes generated by low energy wind waves in the recovery of a beach impacted by extreme events: Nha trang, vietnam. *Journal of Coastal Research*, *70* (sp1).
Marchesiello, P., Kestenare, E., Almar, R., Boucharel, J., & Nguyen, N. M. (2020, November). Longshore drift produced by climate-modulated monsoons and typhoons in the south china sea. *Journal of Marine Systems*, *211*, 103399. Retrieved from `https://doi.org/10.1016/j.jmarsys.2020.103399` doi: 10.1016/j.jmarsys.2020.103399
Melet, A., Almar, R., Hemer, M., Cozannet, G. L., Meyssignac, B., & Ruggiero, P. (2020, August). Contribution of wave setup to projected coastal sea level changes. *Journal of Geophysical Research: Oceans*, *125* (8). Retrieved from `https://doi.org/10.1029/2020jc016078` doi: 10.1029/2020jc016078
Miller, J. K., & Dean, R. G. (2004). A simple new shoreline change model. *Coastal Engineering*, *51*, 531-556.
Montaño, J., Coco, G., Antolínez, J. A. A., Beuzen, T., Bryan, K. R., Cagigal, L., ... Vos, K. (2020, Feb 07). Blind testing of shoreline evolution models. *Scientific Reports*, *10* (1), 2137.
Morton, R. A., Paine, J. G., & Gibeaut, J. C. (1994). Stages and durations of post-storm beach recovery, southeastern texas coast, u.s.a. *Journal of Coastal Research*, *10*, 884-908.
Ondoa, G. A., Almar, R., Jouanno, J., Bonou, F., Castelle, B., & Larson, M. (2020, may). Beach adaptation to intraseasonal sea level changes. *Environmental Research Communications*, *2* (5), 051003. Retrieved from `https://doi.org/10.1088%2F2515-7620%2Fab8705` doi: 10.1088/2515-7620/ab8705
Ondoa, G. A., Bonou, F., Tomety, F., du Penhoat, Y., Perret, C., Degbe, C., & Almar, R. (2017). Beach response to wave forcing from event to inter-annual time scales at grand popo, benin (gulf of guinea). *Water*, *9* (6).
Phillips, M. S., Harley, M. D., Turner, I. L., Splinter, K. D., & Cox, R. J. (2017, March). Shoreline recovery on wave-dominated sandy coastlines: the role of sandbar morphodynamics and nearshore wave parameters. *Marine Geology*, *385*, 146–159. Retrieved from `https://doi.org/10.1016/j.margeo.2017.01.005` doi: 10.1016/j.margeo.2017.01.005
Pianca, C., Holman, R., & Siegle, E. (2015). Shoreline variability from days to decades: Results of long-term video imaging. *Journal Of Geophysical Research Oceans*, *120*, 2159-2178.
Plant, N. G., Aarninkhof, S. G. J., Turner, I. L., & Kingston, K. S. (2007, May). The performance of shoreline detection models applied to video imagery. *Journal of Coastal Research*, *233*, 658–670. Retrieved from

https://doi.org/10.2112/1551-5036(2007)23[658:tposdm]2.0.co;2 doi: 10.2112/1551-5036(2007)23[658:tposdm]2.0.co;2

Ranasinghe, R., McLoughlin, R., Short, A., & Symonds, G. (2004, March). The southern oscillation index, wave climate, and beach rotation. *Marine Geology*, *204*(3-4), 273–287. Retrieved from https://doi.org/10.1016/s0025-3227(04)00002-7 doi: 10.1016/s0025-3227(04)00002-7

Robinet, A., Castelle, B., Idier, D., Harley, M., & Splinter, K. (2020). Controls of local geology and cross-shore/longshore processes on embayed beach shoreline variability. *Marine Geology*, *422*, 106118.

Robinet, A., Idier, D., Castelle, B., & Marieu, V. (2018). A reduced-complexity shoreline change model combining longshore and cross-shore processes: the lx-shore model. *Environ. Model. Softw.*, *109*, 1-16.

Roelvink, D., Reniers, A., van Dongeren, A., van Thiel de Vries, J., McCall, R., & Lescinski, J. (2009, November). Modelling storm impacts on beaches, dunes and barrier islands. *Coastal Engineering*, *56*(11-12), 1133–1152. Retrieved from https://doi.org/10.1016/j.coastaleng.2009.08.006 doi: 10.1016/j.coastaleng.2009.08.006

Smith, R. K., & Bryan, K. R. (2007, July). Monitoring beach face volume with a combination of intermittent profiling and video imagery. *Journal of Coastal Research*, *234*, 892–898. Retrieved from https://doi.org/10.2112/04-0287.1 doi: 10.2112/04-0287.1

Splinter, K. D., Turner, I., Reinhardt, M., & Ruessink, B. (2017). Rapid adjustment of shoreline behaviour to changing seasonality of storms: observations and modelling at an open-coast beach. *Earth Surf. Process. Landf.*, *42*, 1886-1194.

Splinter, K. D., Turner, I. L., & Davidson, M. A. (2013, July). How much data is enough? the importance of morphological sampling interval and duration for calibration of empirical shoreline models. *Coastal Engineering*, *77*, 14–27. Retrieved from https://doi.org/10.1016/j.coastaleng.2013.02.009 doi: 10.1016/j.coastaleng.2013.02.009

Splinter, K. D., Turner, I. L., Davidson, M. A., Patrick, B., Castelle, B., & Oltman–Shay, J. (2014). A generalized equilibrium model for predicting daily to interannual shoreline response. *Geophys. Res. Earth Surf.*, *119*(52), 1936-1958.

Stokes, C., Davidson, M., & Russell, P. (2015). Observation and prediction of three-dimensional morphology at a high-energy macrotidal beach. *Geomorphology*, *243*, 1-13.

Sutherland, J., Peet, A., & Soulsby, R. (2004). Evaluating the performance of morphological models. *Coastal Engineering*, *51*, 917-939.

Takbash, A., & Young, I. R. (2019, September). Global ocean extreme wave heights from spatial ensemble data. *Journal of Climate*, *32*(20), 6823–6836. Retrieved from https://doi.org/10.1175/jcli-d-19-0255.1 doi: 10.1175/jcli-d-19-0255.1

Thuan, D. H., Almar, R., Marchesiello, P., & Viet, N. (2019). Video sensing of nearshore bathymetry evolution with error estimate. *J. Mar. Sci. Eng.*, *7*, 233.

Thuan, D. H., Binh, L. T., Viet, N. T., Hanh, D. K., Almar, R., & Marchesiello, P. (2016). Typhoon impact and recovery from continuous video monitoring: a case study from nha trang beach, vietnam. *Journal of Coastal Research*, *75*(sp1).

Turner, I. L., Harley, M. D., Short, A. D., Simmons, J. A., Bracs, M. A., Phillips, M. S., & Splinter, K. D. (2016, April). A multi-decade dataset of monthly beach profile surveys and inshore wave forcing at narrabeen, australia. *Scientific Data*, *3*(1). Retrieved from https://doi.org/10.1038/sdata.2016.24 doi: 10.1038/sdata.2016.24

van Rijn, L., Walstra, D., Grasmeijer, B., Sutherland, J., Pan, S., & Sierra, J.

(2003). The predictability of cross-shore bed evolution of sandy beaches at the time scale of storms and seasons using process-based profile models. *Coastal Engineering*, *47*, 295-327.

Vitousek, S., Barnard, P. L., Limber, P., Erikson, L., & Cole, B. (2017). A model integrating longshore and cross-shore processes for predicting long-term shoreline response to climate change. *Journal of Geophysical Research: Earth Surface*, *122*(4), 782-806.

Walstra, D. J. R., Reniers, A. J. H. M., Ranasinghe, R., Roelvink, J. A., & Ruessink, B. G. (2012). On bar growth and decay during inter-annual net offshore migration. *Coastal Engineering*, *60*, 190-200.

Walstra, D. J. R., Wesselman, D. A., van der Deijl, E. C., & Ruessink, G. (2016). On the intersite variability in inter-annual nearshore sandbar cycles. *Marine Science and Engineering*, *4*(15).

Wright, L. D., Short, A. D., & Green, M. O. (1985). Short-term changes in the morphodynamic states of beaches and surf zones; an empirical predictive model. *Marine Geology*, *62*(52), 339-364.

Yates, M. L., Guza, R. T., & O'Reilly, W. C. (2009). Equilibrium shoreline response: Observations and modeling. *Journal Of Geophysical Research*, *114*.